Thank you for your careful review and constructive suggestions. These suggestions are quite valuable to us, and help improve our manuscript a lot.

Point-to-point responses

We appreciate the reviewers for their valuable and constructive comments, which are very helpful for the improvement of the manuscript. We have revised the manuscript carefully according to the reviewers' comments. We have addressed the reviewers' comments on a point-to-point basis as below for consideration, where the reviewers' comments are cited in ***black****, and the responses are in* ***blue****.*

Zhang et al. present ship-based MAX-DOAS observations of NO_2, HCHO, BrO, and IO conducted during a Shanghai-Arctic cruise. The study draws three main conclusions: (1) measured trace gas columns show good agreement with satellite products (TROPOMI, GEMS, and GOME-2); (2) elevated BrO levels are associated with air masses that experienced prolonged contact with sea ice; and (3) enhanced IO levels are linked to increased biological activity. Overall, the dataset is valuable and the study addresses timely topics, but the manuscript would benefit from deeper engagement with existing literature and more detailed descriptions of the retrieval methods and associated uncertainties.

Major comments

There is extensive literature spanning several decades on Arctic halogen activation, including so-called “bromine explosion” events and their underlying mechanisms. Given that a substantial portion of this manuscript focuses on enhanced bromine levels in the Arctic, it would strengthen the paper to more thoroughly situate the results within this established context, either in the introduction or in the discussion section.

Relevant examples include:

Pratt et al. (2013), Photochemical production of molecular bromine in Arctic surface snowpack

Swanson et al. (2020), Arctic reactive bromine events occur in two distinct sets of environmental conditions: A statistical analysis of six years of observations

Peterson et al. (2017), Observations of bromine monoxide transport in the Arctic sustained on aerosol particles

Brockway et al. (2024), Tropospheric BrO vertical profiles retrieved across the Alaskan Arctic in springtime.

In particular, a comparison with previous MAX-DOAS observations of BrO in the Arctic would be useful.

Throughout the discussion (e.g., Lines 276, 418, and 515), the manuscript attributes enhanced BrO observed by MAX-DOAS to “bromine explosion” or bromine activation events. Traditionally, these events refer to pronounced enhancements of reactive bromine species during Arctic spring, often associated with significant ozone depletion, with BrO mixing ratios on the order of ~20–40 ppt. By late spring and into summer, when melting begins, gas-phase bromine levels typically decrease to background values, with only occasional enhancements associated with fresh snow (see Jeong et al., Multiphase reactive bromine chemistry during late spring in the Arctic). The mechanisms responsible for bromine activation are known to be strongly seasonally dependent.

The measurements presented here were made during summer, a period when previous studies generally report background BrO levels in the Arctic. In addition, the reported BrO vertical

column densities from MAX-DOAS appear higher than those from previous Arctic DOAS measurements and are approximately a factor of 50 larger than GOME satellite observations. These discrepancies warrant further discussion. For example, do the authors expect the retrieved BrO to be primarily near the surface or distributed aloft? If the signal is dominated by near-surface BrO, what mixing ratios would be implied by the reported VCDs (0.2-0.5×10^{15} molecules.cm^{-2}), and are these values consistent with previous summertime observations?

Previous studies of springtime bromine activation also indicate that sea ice contact duration alone is insufficient to explain observed variability. Other controlling factors include meteorological conditions (e.g., wind speed and boundary layer height), sea ice age, the presence of fresh snow or frost flowers, and particulate bromine. Incorporating these factors into the discussion, alongside sea ice contact time, would provide a more balanced and mechanistic interpretation of the results.

The manuscript would also benefit from explicitly stating the uncertainties and detection limits of the MAX-DOAS retrievals.

Re: Thank you for these very professional comments.

Comment1：

Details regarding the observation periods, locations, techniques, and BrO concentration ranges from previous studies (Brockway et al., 2024; Luo et al., 2018; Peterson et al., 2017; Pratt et al., 2013; Swanson et al., 2020; Wagner et al., 2007) are summarized in Table R1. While prior research indicates that BrO vertical column densities (VCDs) typically reach magnitudes of 10^{14} molecules.cm^{-2} during "bromine explosion" events, our summer measurements (ranging from 0.2 - 0.5×10^{15} molecules.cm^{-2} reflect localized, high-intensity enhancements captured by high-resolution ship-based observations. This comparison and its implications have been incorporated into the revised Introduction.

Table R1. Literature review of BrO observation periods, locations, methods, and peak concentrations.

Relevant research	Observation period	Observation location	Observation method	Maximum BrO concentration
Pratt et al. (2013)	March - April	Alaska	Scanner-DOAS	2.2×10^{14} molecules.cm^{-2}
Swanson et al. (2020)	Entire year	Utqiaġvik	MAX-DOAS	1.5×10^{14} molecules.cm^{-2}
Peterson et al. (2017)	March	Alaska	MAX-DOAS	1.2×10^{14} molecules.cm^{-2}
Brockway et al. (2024)	February - April	Alaska	Airborne Imaging DOAS	40 pmol.mol^{-1}
Luo et al. (2018)	April - May	Ny-Ålesund	MAX-DOAS	5.6×10^{14} molecules.cm^{-2}
Wanger et al. (2007)	June - August	Antarctica	Ship-based MAX-DOAS	12×10^{14} molecules.cm^{-2}
This study	August	Arctic	Ship-based MAX-DOAS	5×10^{14} molecules.cm^{-2}

The following content has been added:

Extensive literature over the past few decades has established the foundation for research on polar halogen activation (Brockway et al., 2024; Luo et al., 2018; Peterson et al., 2017; Pratt et al., 2013; Swanson et al., 2020; Wagner et al., 2007), particularly regarding the distribution and underlying mechanisms of reactive halogens during the polar spring. Specifically, Pratt et al. (2013) confirmed the photochemical production of Br_2 from sunlit snowpack, while Swanson et al. (2020) identified distinct environmental patterns of reactive bromine events through long-term

ground-based observations. However, existing datasets primarily analyze springtime data and are concentrated at stationary sites such as Alert, Utqiaġvik, and Ny-Ålesund. Observational evidence for the summer melt season remains scarce, leaving the evolution mechanisms of the halogen cycle under continuous high-radiation conditions unclear.

Comment 2：

We appreciate the reviewer's constructive suggestions regarding the seasonal dependence of BrO concentrations. In this study, we have established an automated quality control (QC) process of "layer-by-layer filtering and progressive evaluation" to ensure the reliability of the MAX-DOAS retrieval results.

Level 1 QC: Basic signal and global fit evaluation. This stage aims to eliminate data with fundamental defects.

$$\mathrm{SNR} = \frac{\text{Maximum of Analysis Signal}}{\text{Maximum of Residual Signal}} \tag{1}$$

$$\mathrm{RMS} = \sqrt{\frac{\sum r_i^2}{N}} \tag{2}$$

The signal-to-noise ratio (SNR) is defined as the ratio of the maximum BrO differential absorption signal to the maximum residual signal, while the root mean square (RMS) is used to evaluate the overall deviation between the model and the measured spectra.

Level 2 QC: Feature-based specific verification. For weak absorbers such as BrO, global metrics (SNR and RMS) may not fully reflect the fitting performance in key spectral bands. Therefore, the coefficient of determination (COD) is introduced.

$$\mathrm{COD} = 1 - \frac{n-1}{n-p} \cdot \frac{SS_{res}}{SS_{tot}} \tag{3}$$

Where, SS_{res} is the sum of residual squares, SS_{tot} is the total variation, n is the number of data points, and p is the number of parameters. By applying strict thresholds (SNR > 1.5, RMS < 0.003, and COD > 0.6), 68.71% of the data were retained. Six sets of BrO fitting results are shown in Figure R1. In summary, the retrieved BrO concentrations do not originate from background noise or fitting errors. This two-level QC system, especially the feature-band-based COD filtering, proves that our retrieved BrO concentrations are real and reliable.

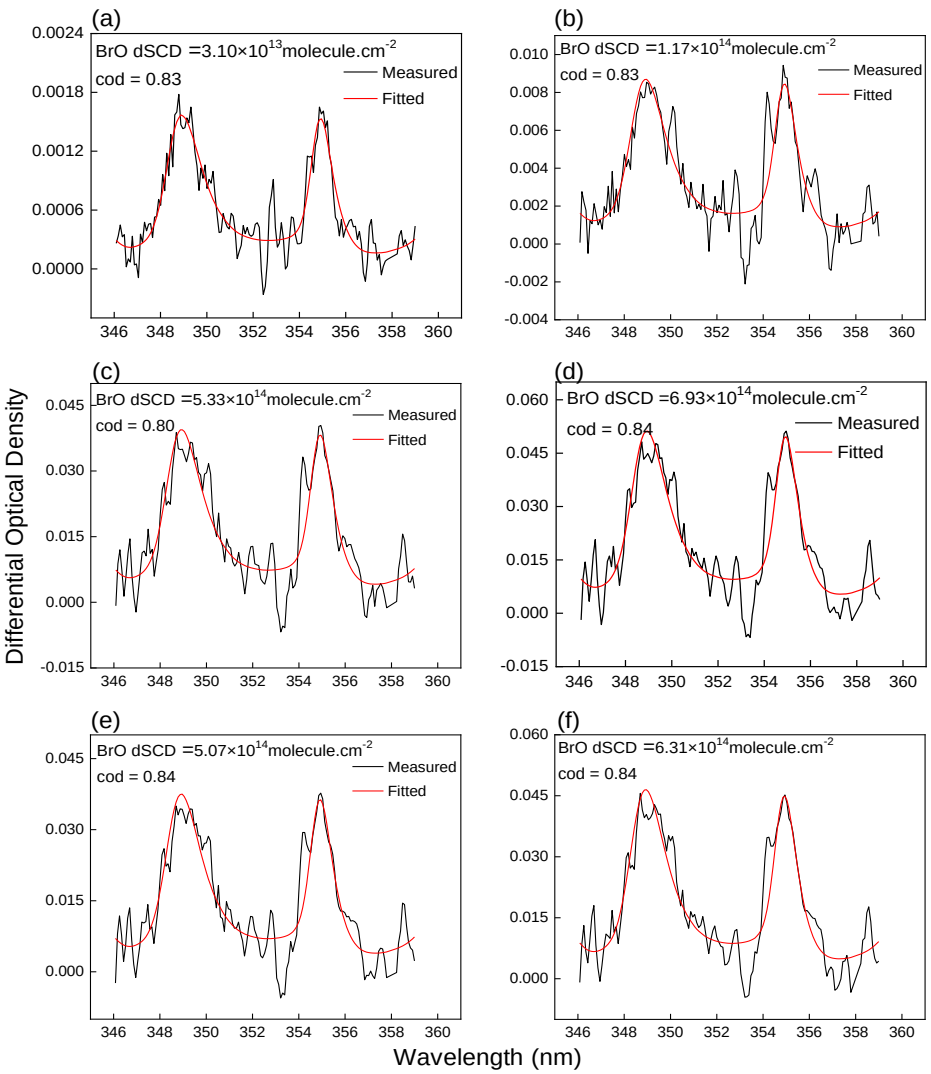

Figure R1. Representative examples of BrO absorption spectral fitting during the observation period.

The retrieval uncertainty of the MAX-DOAS measurements is attributed to four primary sources (Hendrick et al., 2007; Song et al., 2023; Tack et al., 2015; Wagner et al., 2007; Wittrock et al., 2004). First, spectral noise and fitting errors, representing the statistical uncertainty of the DOAS fit, remain within 5% to 10% for NO_2, HCHO, BrO, and IO under clear-sky conditions. Second, the uncertainty in the zenith reference spectrum (ZRS) contributes approximately 10% to 15%. Although subtracting the sequential ZRS from off-axis measurements is intended to cancel stratospheric absorption, residual trace gas abundances in the ZRS (due to stratospheric background or localized tropospheric contamination) can introduce systematic biases. Third, algorithmic uncertainties related to the radiative transfer model (including aerosol vertical distribution, multiple scattering, and profile assumptions) result in an estimated air mass factor (AMF) uncertainty of 10% to 20%. Sensitivity tests specifically conducted for the Arctic sea-ice environment indicate that surface albedo has a negligible impact on boundary layer observations at low elevation angles. Finally, errors arising from stratospheric gradients and atmospheric inhomogeneity are maintained below 10% by employing the sequential ZRS method and restricting the solar zenith angle (SZA) to less than 75°.

Consequently, the total combined uncertainty for the retrieved VCDs ranges from 18.1% to

28.7%. Note that this relative uncertainty may increase in the pristine Arctic atmosphere when tropospheric concentrations approach detection limits. A detailed breakdown of these uncertainties is provided in Table R2.

Table R2. MAX-DOAS retrievals uncertainty

Error sources	Estimated Uncertainty
Smoothing and Noise Error	5%-10%
Uncertainty of the reference spectrum	10%-15%
Algorithm Error	10%–20%
Errors from Stratospheric Gradient and Atmospheric Inhomogeneity	10%

Comment 3：

A statistical comparison indicates that MAX-DOAS BrO concentrations are 1.05 to 11.57 times those of GOME observations. As shown in Figure R2, ratios of 5 or less account for 74.69% of the total, while ratios exceeding 5 represent 25.31%. This difference is primarily due to the following reasons. Initially, the coarse spatial resolution of GOME (40 × 40 km) leads to a significant dilution effect compared to the localized footprint of ship-based MAX-DOAS. Consequently, sub-grid scale emission hotspots, such as those from sea ice leads or frost flowers, are effectively smeared out in the satellite's spatial average (Pinardi et al., 2020; Seo et al., 2020). Furthermore, while satellite retrievals are often constrained by clouds and sea ice variability, MAX-DOAS provides enhanced sensitivity to boundary layer BrO through its extended effective light paths in the lower troposphere (Seo et al., 2020; Theys et al., 2011).

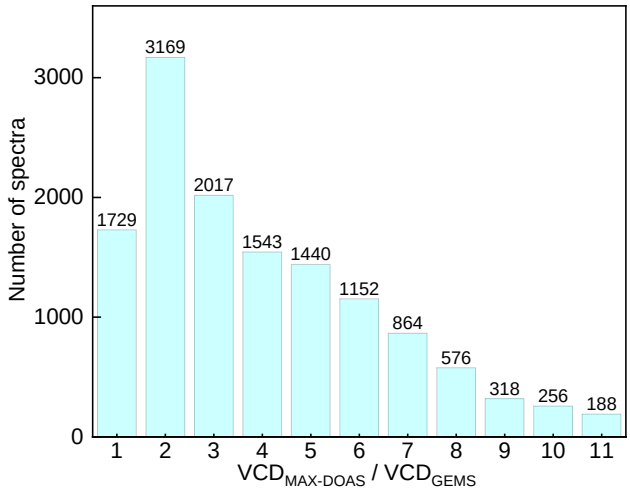

Figure R2. Frequency distribution histogram of the ratios of ship-based MAX-DOAS to GOME satellite BrO concentrations.

The MAX-DOAS measurements in this study were conducted at elevation angles (EAs) of 10° and 20°, with the observed BrO predominantly concentrated within the near-surface layer. Because the restricted set of EAs precludes a formal profile inversion, we utilized a parameterized exponential decay model to estimate the surface mixing ratio.

$$c(z) = c_0 \cdot \exp(-z / H) \quad (4)$$

In this model, c_0 denotes the surface number density and H represents the effective scale height. The surface number density was derived from the VCD using the following relationship:

$$c_0 = \frac{VCD}{H} \quad (5)$$

Following previous studies (Peng et al., 2023; Shupe et al., 2013), the effective scale height for the Arctic boundary layer was set to 500 m. Under this assumption, our observed VCDs ($0.2\text{-}0.5\times10^{15}$ molecules.cm^{-2}) correspond to surface mixing ratios between 8 and 20 ppt. These values are elevated relative to other summer observations in the Arctic, which generally range from 3 to 5 ppt (Bognar et al., 2020; Burd et al., 2017; Hurlock et al., 2007). Two primary factors may explain this discrepancy. First, the idealized exponential decay assumption may introduce an inherent upward bias in the estimated mixing ratios. Second, our cruise specifically sampled the marginal ice zone, polynyas, and sea ice leads. Even as regional temperatures rise during the Arctic summer, surface temperatures in high-concentration ice zones often remain near the freezing point. These sustained low-temperature conditions facilitate active heterogeneous reactions on sea salt aerosols and ice surfaces, thereby driving localized bromine activation (Eicken et al., 2002; Richter et al., 1998; Tremblay et al., 2019).

The retrieval uncertainty of the MAX-DOAS measurements is attributed to four primary sources (Hendrick et al., 2007; Song et al., 2023; Tack et al., 2015; Wagner et al., 2007; Wittrock et al., 2004). First, spectral noise and fitting errors, representing the statistical uncertainty of the DOAS fit, remain within 5% to 10% for NO_2, HCHO, BrO, and IO under clear-sky conditions. Second, the uncertainty in the zenith reference spectrum (ZRS) contributes approximately 10% to 15%. Although subtracting the sequential ZRS from off-axis measurements is intended to cancel stratospheric absorption, residual trace gas abundances in the ZRS (due to stratospheric background or localized tropospheric contamination) can introduce systematic biases. Third, algorithmic uncertainties related to the radiative transfer model (including aerosol vertical distribution, multiple scattering, and profile assumptions) result in an estimated air mass factor (AMF) uncertainty of 10% to 20%. Sensitivity tests specifically conducted for the Arctic sea-ice environment indicate that surface albedo has a negligible impact on boundary layer observations at low elevation angles. Finally, errors arising from stratospheric gradients and atmospheric inhomogeneity are maintained below 10% by employing the sequential ZRS method and restricting the solar zenith angle (SZA) to less than 75°.

Consequently, the total combined uncertainty for the retrieved VCDs ranges from 18.1% to 28.7%. Note that this relative uncertainty may increase in the pristine Arctic atmosphere when tropospheric concentrations approach detection limits. A detailed breakdown of these uncertainties is provided in Table R2.

Comment 4:

We appreciate the reviewer's constructive feedback regarding additional drivers of BrO variability, such as meteorological parameters (wind speed and boundary layer height), sea ice age, the presence of fresh snow or frost flowers, and particulate bromine. To address these points, we incorporated key environmental datasets for August 2021 from the European Centre for Medium-Range Weather Forecasts (ECMWF) and the National Snow and Ice Data Center (NSIDC). These parameters, including boundary layer height, wind speed, snow density, snowfall,

and sea ice age, allowed for a detailed discussion on how the physical environment modulates BrO levels. Regarding frost flowers, available records in public databases are currently limited to May 2020, providing insufficient spatio-temporal coverage for our study period. Additionally, as the determination of polar particulate bromine generally requires specialized in situ sampling (Hara et al., 2002, 2018), no publicly accessible datasets exist for our specific observation area. These data limitations preclude a rigorous quantitative assessment of the individual contributions of frost flowers and particulate bromine to the observed BrO response mechanisms.

1. Influence of boundary layer height:

Following your recommendation, we analyzed the spatial distribution of the Arctic boundary layer height (BLH) for August 2021 using ECMWF data (see Figure R3, included in the Supplement). Vertical coupling is a fundamental prerequisite for observing the bromine cycle. Prior research indicates that MAX-DOAS sensitivity to BrO is altitude-dependent, typically exhibiting higher weighting within the middle and upper boundary layer. Consequently, significant enhancement signals are detectable only when active bromine released from the sea-ice surface is transported into these layers via effective vertical mixing (Frieß et al., 2011; Peterson et al., 2017; Simpson et al., 2017; Wagner et al., 2007). Furthermore, the BLH serves as a physical barrier to vertical transport. If a back-trajectory altitude exceeds the real-time BLH, the vertical flux of active bromine from the surface is inhibited, preventing its entry into the air mass transport path. In such instances, contact with sea ice does not contribute to the observed BrO enhancements (Jacobi et al., 2010; Moore et al., 2014; Roberts et al., 2014; Simpson et al., 2017; Wagner et al., 2007).

To refine our analysis, we implemented spatio-temporally synchronized BLH as a dynamic constraint. This approach filters out invalid high-altitude trajectories, ensuring that the sea-ice contact time accurately represents the material exchange between the air mass and its source region. Following this refinement, the correlation between tropospheric BrO concentrations and sea-ice contact time improved to 0.77 (Figure R4). This result underscores the critical role of boundary layer dynamics in modulating the transmission of polar "bromine explosion" signals. A comprehensive discussion regarding these boundary layer effects has been incorporated into the revised manuscript.

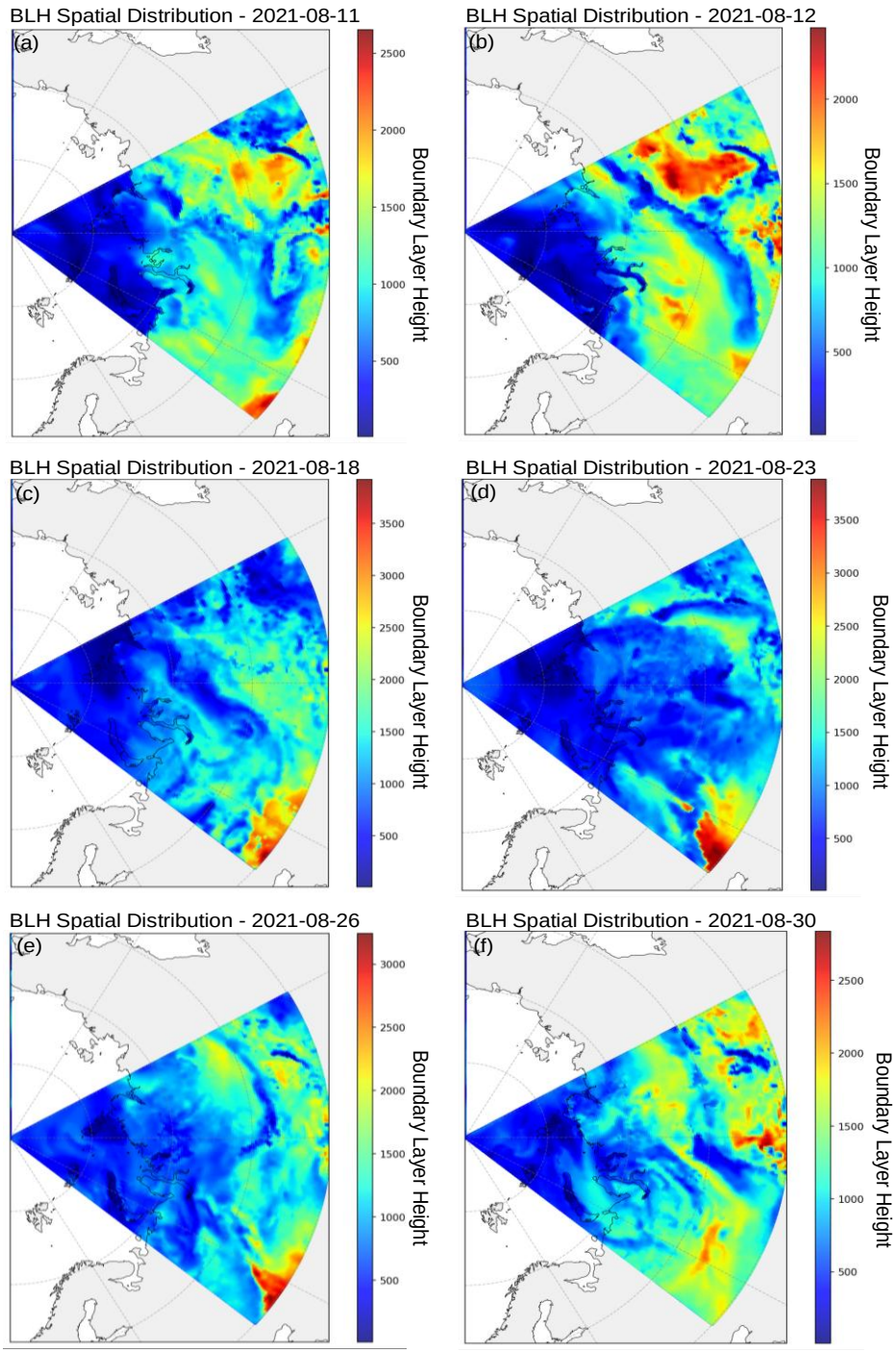

Figure R3. Spatial distribution of Boundary Layer Height (BLH) in the Arctic during August 2021.

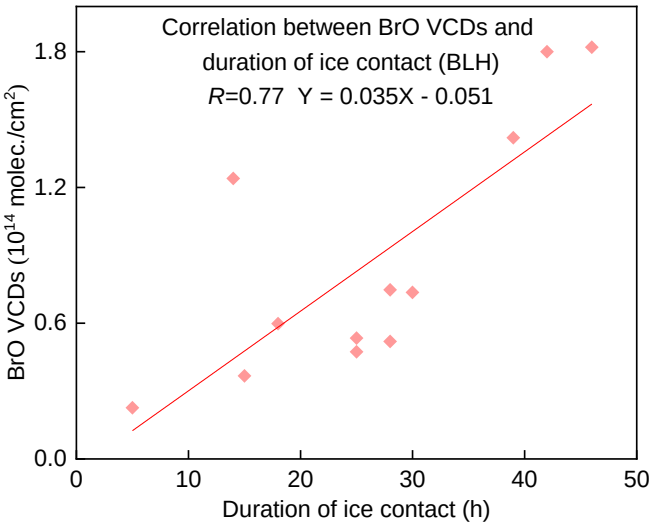

Figure R4. Correlation analysis between tropospheric BrO concentration and sea ice contact time under boundary layer height (BLH) constraint.

The following content has been added:

To refine the quantification of material exchange between air masses and surface sources, we incorporated the boundary layer height (BLH) as a dynamic constraint for calculating sea-ice contact time. Utilizing ECMWF data for August 2021 (see Supplement Fig. S10), we coupled spatio-temporally synchronized BLH values with air mass back-trajectories. Specifically, a trajectory point was categorized as "effective sea-ice contact" only if its altitude simultaneously satisfied two conditions: being below 200 m and below the real-time BLH. This dual criterion ensures that contact occurs within the mixed layer, where surface-released reactive bromine can physically interact with the air mass via turbulent transport.

Following the integration of the BLH constraint, the correlation between tropospheric BrO concentrations and sea-ice contact time improved significantly to 0.77 (see Supplement Fig. S11). This enhancement stems from two primary factors. First, MAX-DOAS instruments typically exhibit peak vertical sensitivity within the middle and upper boundary layer (Frieß et al., 2011; Peterson et al., 2017; Simpson et al., 2017; Wagner et al., 2007). Consequently, surface emissions must undergo effective vertical mixing to reach these altitudes and be detected by the instrument. Second, the BLH serves as a physical barrier to vertical transport. If a back-trajectory altitude exceeds the local BLH, the upward flux of reactive bromine is inhibited, preventing its entrainment into the air mass. In such instances, contact with sea ice does not contribute to the observed BrO enhancements (Frieß et al., 2011; Peterson et al., 2017; Simpson et al., 2017; Wagner et al., 2007).

2. Influence of Wind Direction:

In response to the reviewer's recommendation, we analyzed the spatial distribution of Arctic wind directions for August 2021 using ECMWF data (see Figure R5, included in the Supplement). The results reveal that BrO variability is highly sensitive to prevailing wind regimes. Specifically, under southwesterly (SW) flow, the correlation between tropospheric BrO and sea-ice contact time reaches 0.84, suggesting that bromine levels are predominantly driven by surface-level contact. Under southeasterly (SE) conditions, however, this correlation decreases to 0.65 (Figure R6).

These observations align with previous studies (Bognar et al., 2020; May et al., 2016; Nilsson et al., 2001), which demonstrate that wind direction serves as a proxy for varying air mass source regions and transport histories. SW winds likely correspond to air masses with more direct sea-ice origins, where the bromine activation mechanism is predominantly governed by the duration of sea-ice contact (Bognar et al., 2020; Brockway et al., 2024; Seo et al., 2020), resulting in a more explicit relationship. Conversely, the SE wind regime may involve more vigorous atmospheric turbulence or enhanced aerosol cycling. In such cases, BrO concentrations depend more heavily on heterogeneous recycling on sea salt aerosol surfaces rather than being solely driven by direct surface contact (Bognar et al., 2020; Brockway et al., 2024; Seo et al., 2020). A comprehensive discussion of these wind-directional effects has been incorporated into the revised manuscript.

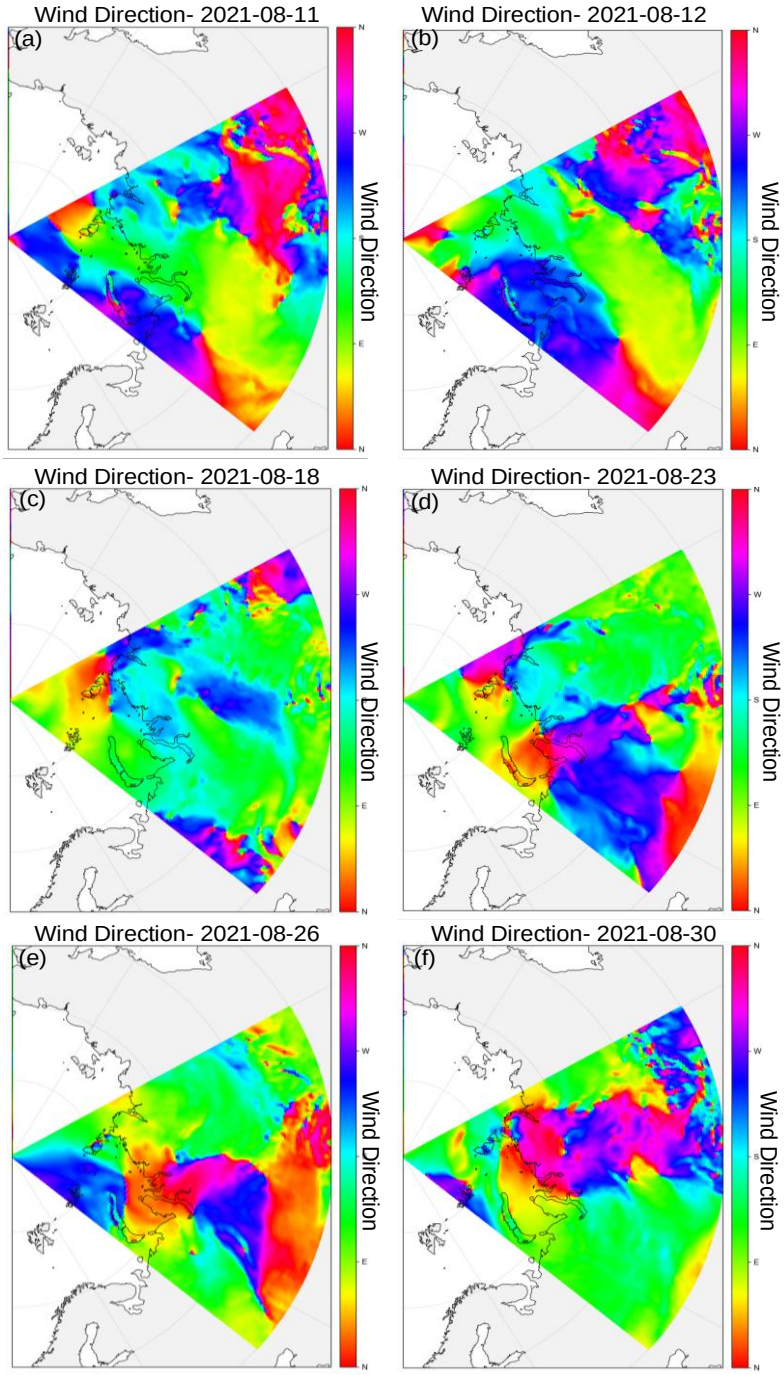

Figure R5. Spatial distribution of wind direction in the Arctic during August 2021.

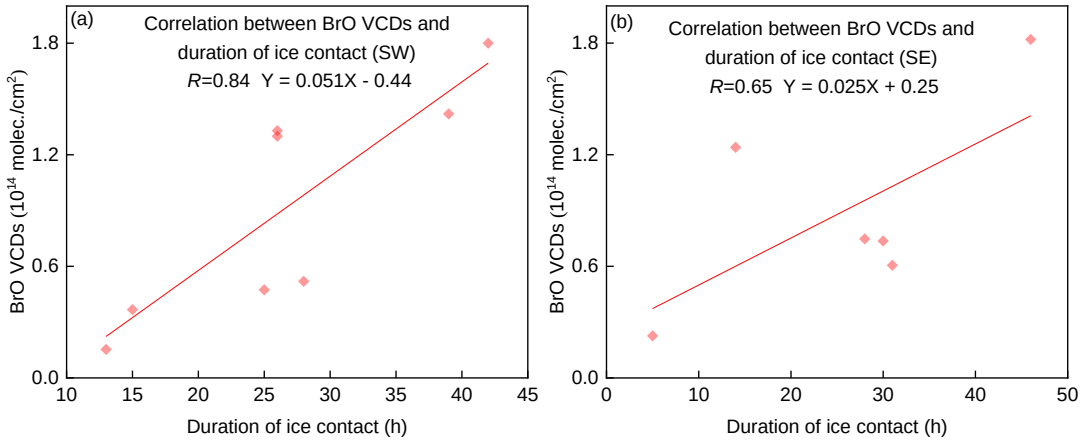

Figure R6. Correlation analysis between tropospheric BrO concentration and sea ice contact time under wind direction constraint. (a) southwest wind direction, (b)southeast wind direction

The following content has been added:

Our study identifies a significant modulating role of wind direction on BrO variability. Utilizing ECMWF datasets, we analyzed the spatial distribution of Arctic wind directions for August 2021 (see Supplement Fig. S12). The findings reveal that the study area was predominantly influenced by southwesterly (SW) and southeasterly (SE) wind regimes. Under SW flow, the correlation coefficient (R) between BrO and sea-ice contact time reached 0.84, whereas SE conditions exhibited a weaker correlation of 0.65 (see Supplement Fig. S13). This spatial heterogeneity reflects how air mass trajectories dictate specific bromine activation mechanisms. The robust correlation under SW winds likely stems from airflows originating from high-salinity first-year ice (FYI) zones. These pathways are relatively stable and primarily governed by heterogeneous release from ice surfaces (Bognar et al., 2020; Brockway et al., 2024; Seo et al., 2020). In contrast, the reduced correlation under SE winds suggests that air masses encounter more complex physicochemical interference during transport (Bognar et al., 2020; Brockway et al., 2024; Seo et al., 2020). For instance, Bognar et al.(2020) observed at the Eureka station that cyclonic activity and intense atmospheric disturbances can shift BrO sources toward heterogeneous recycling on sea salt aerosol surfaces, decoupling the concentrations from simple surface contact processes.

3. Influence of Sea Ice Age:

In response to the reviewer's comment, we analyzed the spatial distribution of Arctic sea ice age between July 31 and September 3, 2021, using NSIDC data (see Figure R7, included in the Supplement). Integrating air mass back-trajectories with geographical coordinates, we determined that the sea ice encountered during the August 2021 observation period was predominantly composed of first-year ice (FYI, age ≤ 1). FYI is characterized by high initial salinity (typically 50‰ to 100‰), providing an abundant substrate for reactive bromine activation (Bognar et al., 2020; Frieß et al., 2004; Simpson et al., 2007). Conversely, multi-year ice (MYI) often undergoes significant desalination due to summer brine drainage, with salinity typically decreasing to 5‰ to 10‰. This reduction in salinity renders MYI a less efficient source of reactive bromine.

The robust correlation (R = 0.73) observed between BrO and sea-ice contact time is primarily

explained by the consistent presence of highly active FYI along the air mass pathways. This finding aligns with Simpson et al. (2007), who identified contact time with FYI as the most reliable predictor of BrO concentrations in the Arctic. A comprehensive discussion on these sea-ice age effects and their implications for bromine activation has been incorporated into the revised manuscript.

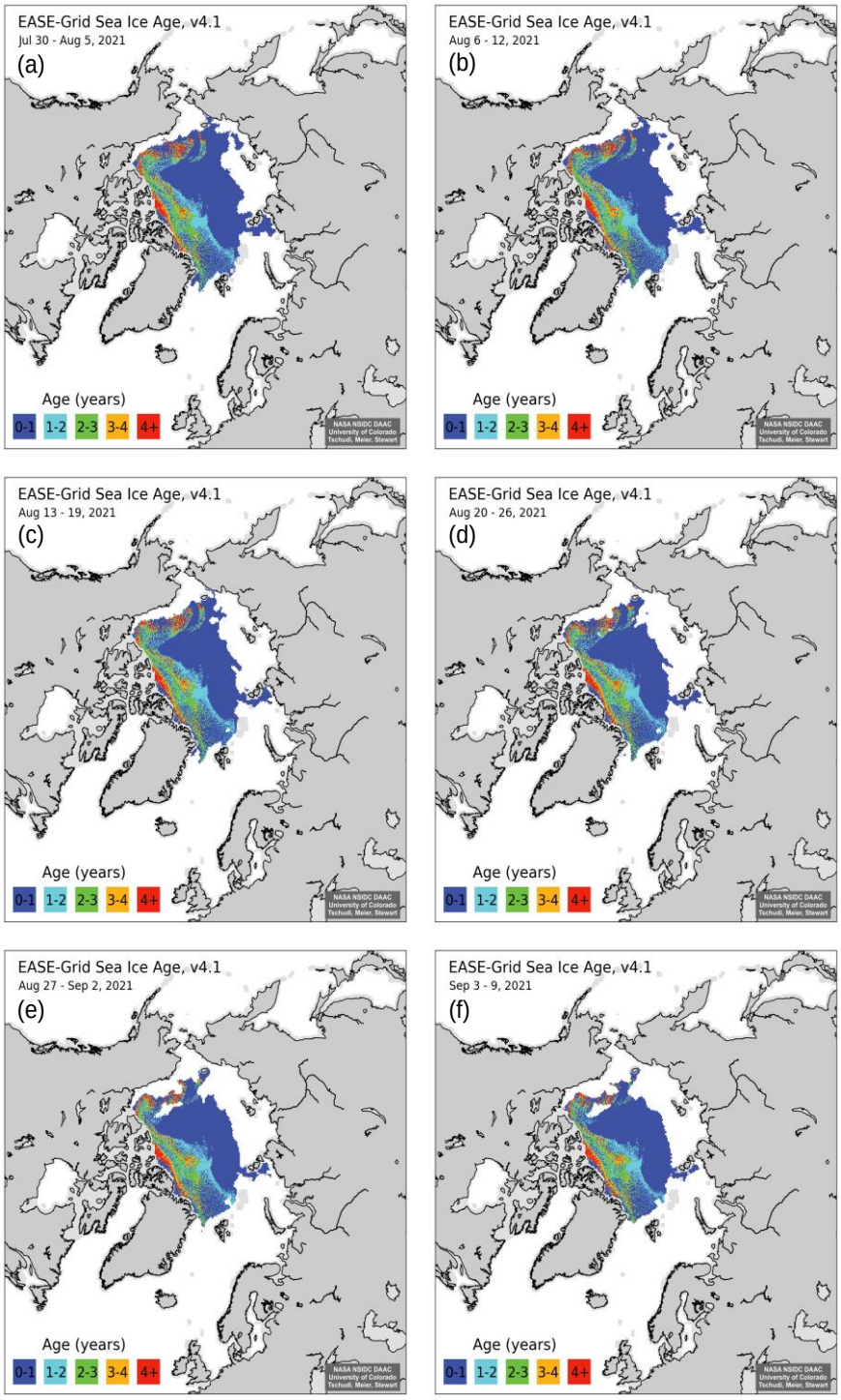

Figure R7. Correlation analysis between tropospheric BrO concentration and sea ice contact time under sea ice age constraint. (Data source: daacdata.apps.nsidc.org)

The following content has been added:

To further explore the drivers of BrO activation, we incorporated spatial data on sea ice age (sourced from daacdata.apps.nsidc.org). Analysis for the period from July 31 to September 3, 2021, reveals that the sea ice along the cruise track and within the air mass back-trajectories consisted predominantly of first-year ice (FYI, age ≤ 1), as illustrated in the Supplement Fig. S14.

Sea ice age significantly modulates the heterogeneous release of bromine, as younger ice typically exhibits higher surface salinity than multi-year ice (MYI) due to the process of brine expulsion (Bognar et al., 2020; Frieß et al., 2004; Simpson et al., 2007). Notably, Simpson et al. (2007) demonstrated that the duration of contact with FYI is a more reliable predictor of atmospheric BrO levels than contact with potential frost flowers. Similarly, Frieß et al. (2004) excluded MYI from their Antarctic study because its low salinity was insufficient to sustain effective bromine activation. The robust correlation (R = 0.73) observed between BrO and sea-ice contact time in this study aligns with these previous reports. Since the sampled air masses primarily interacted with high-salinity FYI, the abundant supply of bromide ions facilitated the "bromine explosion" mechanism, establishing sea-ice contact time as the primary driver of the observed BrO variability.

4. Influence of Snow Density:

In response to the reviewer's suggestion, we analyzed the spatial distribution of Arctic snow density for August 2021 using ECMWF data (see Figure R8, included in the Supplement). Integrating these data with air mass back-trajectories, we found that snow density remained remarkably stable across the sampled regions, exhibiting negligible variability (less than 1E-5) around a mean of 100.0 kg/m^3. As a fundamental determinant of snow porosity and permeability, density dictates the efficiency of brine migration from the sea-ice interface to the snowpack surface, thereby influencing heterogeneous reaction rates (Abbatt et al., 2012; Domine et al., 2008). The spatial uniformity of snow density across the study area suggests that the physical structure of the snowpack provides a consistent contribution to bromine activation along all trajectory paths. A comprehensive discussion regarding the role of snow density in modulating bromine chemistry has been incorporated into the revised manuscript.

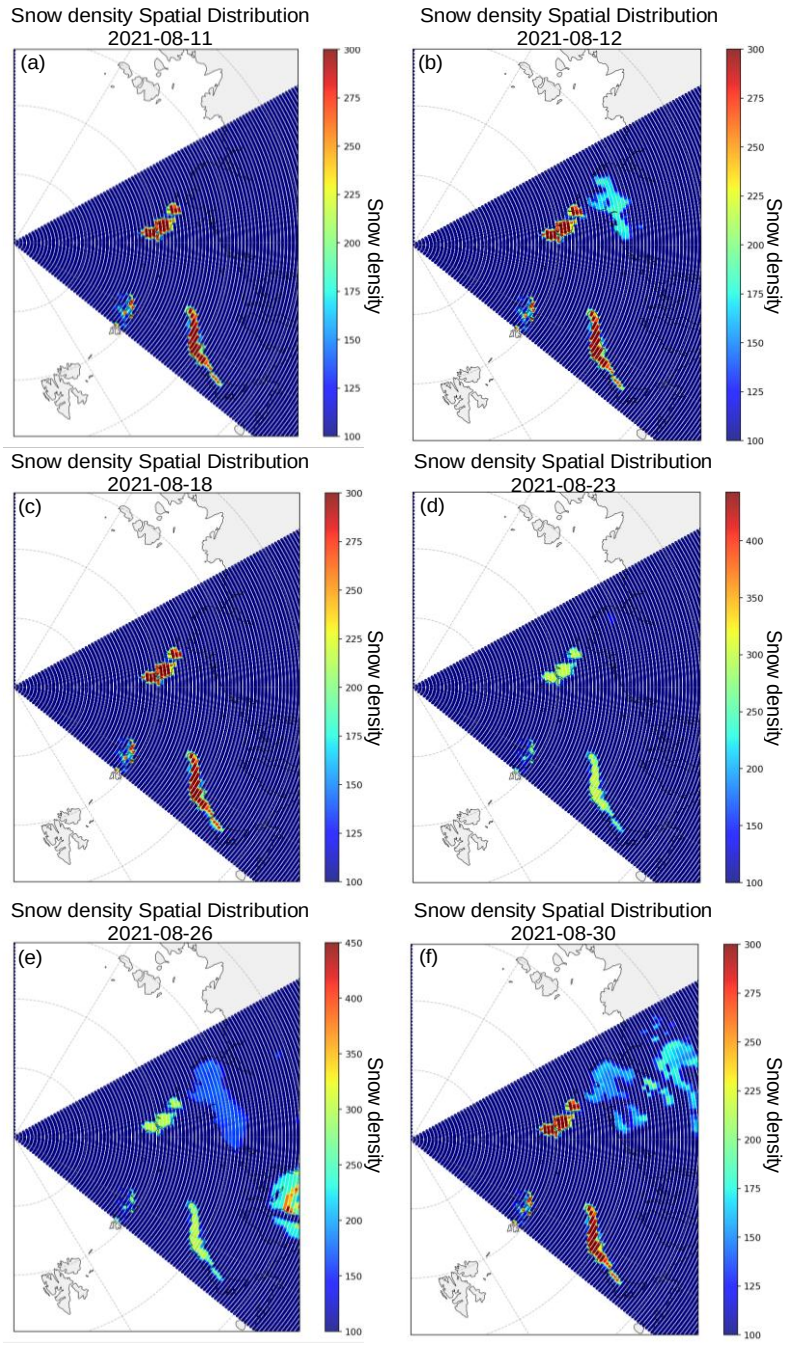

Figure R8. Correlation analysis between tropospheric BrO concentration and sea ice contact time under snow density constraint.

The following content has been added:

Snowpack density is a fundamental physical parameter that determines porosity and permeability, thereby influencing brine migration from the sea-ice interface to the snow surface and the overall efficiency of heterogeneous reactions (Abbatt et al., 2012; Domine et al., 2008). In this study, we characterized the spatial distribution of snow density across the survey region using ECMWF data (see Supplement Fig. S15). By integrating geographical coordinates with air mass back-trajectories, we observed that snow density remained remarkably stable throughout the study area. Fluctuations were negligible, staying below 1E-5 around a mean value of 100.0 kg/m^3. Such

spatial homogeneity suggests that the physical structure of the snowpack provided a consistent contribution to bromine activation along all sampled trajectory paths.

5. Influence of Snowfall:

Following the reviewer's recommendation, we utilized ECMWF data to analyze the spatial distribution of Arctic snowfall for August 2021 (see Figure R9, included in the Supplement). Snowfall serves as a critical meteorological forcing that alters both surface characteristics and atmospheric loading (Bognar et al., 2020; Burd et al., 2017; Frey et al., 2020; Peterson et al., 2017; Pratt et al., 2013). To evaluate its impact, we categorized the observations into snow-free (Snowfall = 0) and active snowfall (Snowfall > 0) periods.

Correlation analysis (Figure R10) indicates that while a robust correlation (R = 0.87) exists under snow-free conditions, this relationship weakens significantly (R = 0.61) during snowfall events. Several mechanisms may explain this divergence. Initially, the accumulation of fresh snow can physically mask bromine-rich substrates, such as saline snowpacks on first-year ice or frost flowers, which suppresses the heterogeneous release of reactive bromine into the atmosphere (Burd et al., 2017; Pratt et al., 2013). Additionally, wet deposition during snowfall events efficiently removes reactive bromine species and recycling aerosols from the air, decoupling BrO concentrations from simple sea-ice contact durations (Frey et al., 2020; Peterson et al., 2017). Finally, as highlighted by Bognar et al. (2020), snowfall in the Arctic is frequently associated with cyclonic systems. The resulting high winds and boundary layer instabilities trigger vigorous vertical mixing, shifting BrO variability from a regime dominated by surface contact to one governed by complex, nonlinear multivariable dynamics. A comprehensive discussion of these snowfall-induced effects has been incorporated into the revised manuscript.

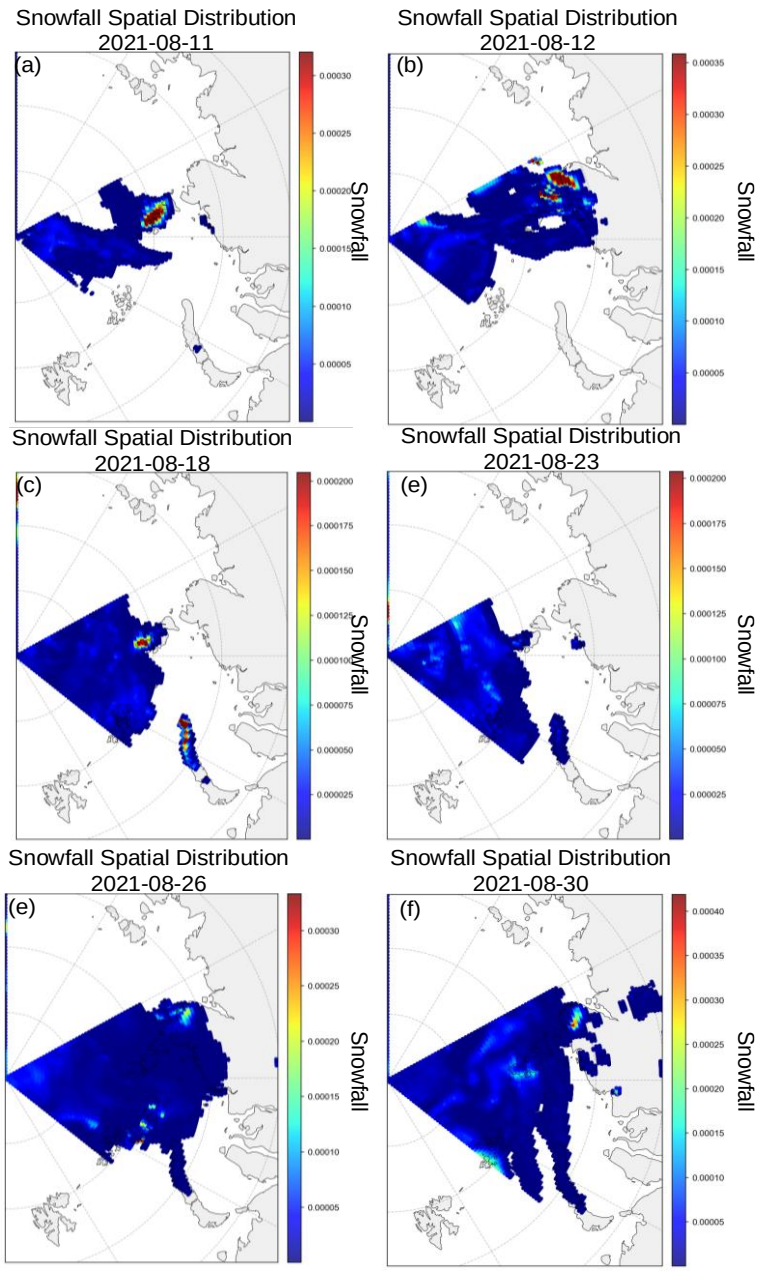

Figure R9. Correlation analysis between tropospheric BrO concentration and sea ice contact time under snowfall constraint.

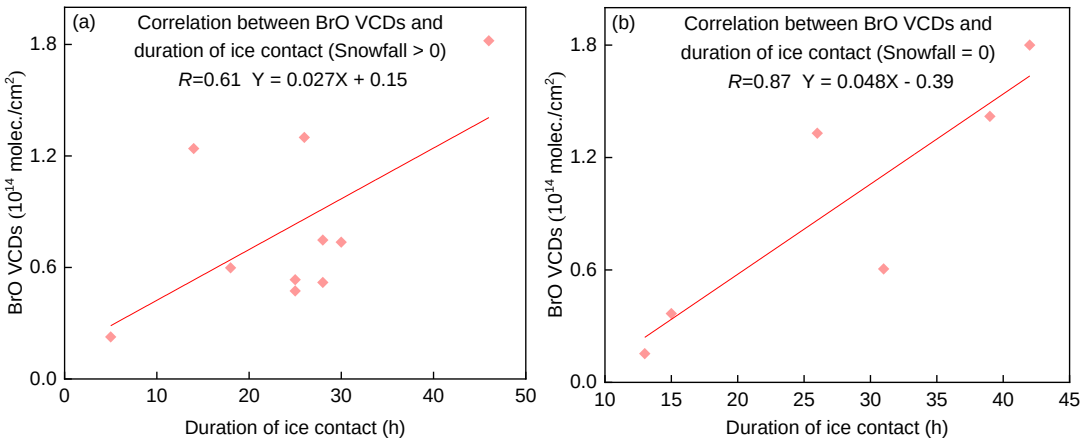

Figure R10. Correlation analysis between tropospheric BrO concentration and sea ice contact time under snowfall. (a) snowfall > 0, (b)snowfall = 0.

The following content has been added:

As a critical meteorological forcing that alters polar surface characteristics and atmospheric loading (Bognar et al., 2020; Burd et al., 2017; Frey et al., 2020; Peterson et al., 2017; Pratt et al., 2013), snowfall significantly modulates BrO variability. In this study, we analyzed the spatial distribution of Arctic snowfall for August 2021 based on ECMWF data (see Supplement Fig. S16). To evaluate the modulating role of snowfall, we partitioned the observations into snow-free (Snowfall = 0) and active snowfall (Snowfall > 0) periods. The resulting correlations between BrO and sea-ice contact time are illustrated in the Supplement Fig. S17.

Our analysis indicates that while a robust correlation (R = 0.87) exists under snow-free conditions, this relationship weakens to R = 0.61 during snowfall events. Several mechanisms likely drive this divergence. Initially, the accumulation of fresh snow can physically mask bromine-rich substrates, such as saline snowpacks on first-year ice or frost flowers, which suppresses the heterogeneous release of reactive bromine into the atmosphere (Bognar et al., 2020; Burd et al., 2017; Frey et al., 2020; Peterson et al., 2017; Pratt et al., 2013). Additionally, wet deposition during snowfall efficiently removes reactive bromine species and recycling aerosols from the air, decoupling BrO concentrations from simple sea-ice contact durations (Bognar et al., 2020; Burd et al., 2017; Frey et al., 2020; Peterson et al., 2017; Pratt et al., 2013). Finally, as noted by Bognar et al. (2020), snowfall in the Arctic is frequently coupled with cyclonic activity. The resulting high winds and boundary layer instabilities trigger vigorous vertical mixing, shifting BrO variability from a regime dominated by surface contact to one governed by complex, non-linear multivariable dynamics.

6. Relative Contributions of Environmental Drivers to BrO Variability:

To quantitatively assess the relative contributions of environmental factors to BrO variability while accounting for non-linear atmospheric processes, we implemented a Generalized Additive Model (GAM). The model utilized BrO concentrations as the dependent variable, with sea-ice contact time, snowfall, boundary layer height (BLH), and wind direction as predictors. Parameters that remained invariant during the campaign, specifically sea ice age and snow density, were omitted. As illustrated in Figure R11, the model achieved an overall correlation of R = 0.80.

Our findings identify sea-ice contact duration as the primary driver of BrO enhancements, contributing 48.63% independently. This result provides quantitative evidence for the predominance of sea-ice surface chemistry in driving the observed bromine activation. Snowfall accounts for 8.81% of the variability, with partial effect analysis suggesting a complex modulation that likely involves competition between physical scavenging and surface activation. While the direct contributions of wind direction (3.77%) and BLH (3.42%) are relatively low, the observed shifts in correlation (e.g., R = 0.87 during snow-free periods versus R = 0.61 during snowfall) indicate that meteorological forcing primarily governs the "activation efficiency" of sea-ice contact by altering boundary layer stability and air mass trajectories. The remaining unexplained variance (35.37%) is likely linked to unmeasured parameters. This GAM-based quantitative assessment and the associated discussion of nonlinear mechanisms have been incorporated into the revised manuscript.

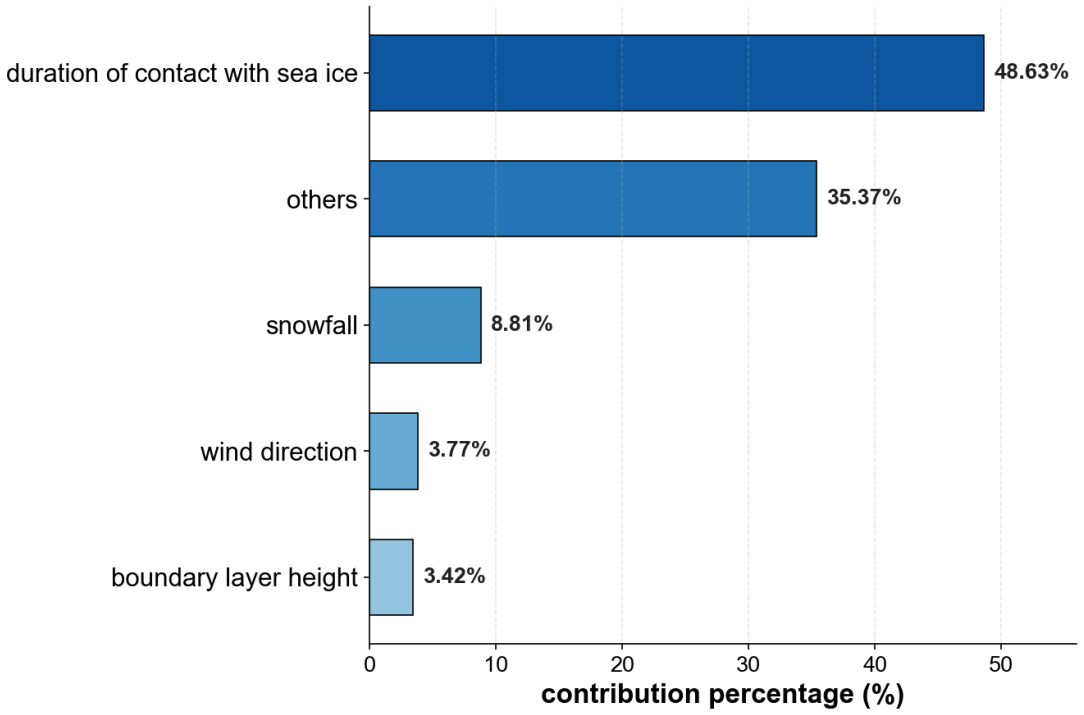

Figure R11. Quantitative assessment of factors influencing BrO enhancement based on the Generalized Additive Model.

The following content has been added:

To elucidate the synergistic impacts of environmental parameters and quantify their respective contributions to bromine activation, we employed a Generalized Additive Model (GAM) to investigate BrO variability (see Supplement Fig. S9). The model achieved an overall correlation of R = 0.80. Our quantitative assessment identifies sea-ice contact time as the primary driver of BrO enhancements, accounting for an independent contribution of 48.63%. This finding statistically verifies that surface contact is the fundamental requirement for bromine activation and subsequent accumulation. Snowfall contributes 8.81% to the variance, where its negative correlation reflects the physical masking of saline source regions (e.g., frost flowers or salty snowpacks) by fresh snow, thereby inhibiting heterogeneous chemical reactions. While the direct contributions from wind direction (3.77%) and boundary layer height (3.42%) are modest, comparative sub-group analysis (e.g., R = 0.87 for snow-free periods versus R = 0.61 during snowfall) indicates that meteorological forcing primarily governs the intensity and efficiency of "bromine explosions" by modulating boundary layer stability and air mass trajectories (Bognar et al., 2020). The remaining unexplained variance (35.37%) is likely associated with environmental drivers not captured in the current model.

Comment 5：

In response to the reviewer's request for a clear description of the MAX-DOAS retrieval uncertainty, we refer to previous studies (Hendrick et al., 2007; Song et al., 2023; Tack et al., 2015; Wagner et al., 2007; Wittrock et al., 2004). The retrieval uncertainty in this study is categorized into four primary sources. 1) Smoothing and noise errors: These errors stem from statistical uncertainties during the DOAS fitting process. Under clear-sky conditions, fitting errors for NO_2, HCHO, BrO, and IO are within the 5%–10% range. 2) Reference spectrum uncertainty:

Tropospheric Differential Slant Column Densities (DSCDs) are calculated by subtracting a sequential zenith reference spectrum (ZRS) from off-axis measurements ($SCD_{off-axis} - SCD_{90°}$). This assumes that stratospheric absorption cancels out between the two geometries. However, uncertainties in residual trace gas amounts in the ZRS (from stratospheric background or tropospheric pollution) can lead to systematic biases, estimated at approximately 10%–15%. 3) Algorithmic errors: These mainly arise from uncertainties in aerosol vertical distribution, multiple scattering simulations, and profile assumptions within the radiative transfer model. For the Arctic sea-ice environment, sensitivity tests show that surface albedo has a minor impact on boundary layer species at low elevation angles, with the total Air Mass Factor (AMF) uncertainty estimated at 10%–20%. 4) Errors from stratospheric gradients and atmospheric inhomogeneity: Since we employed the sequential ZRS method and filtered for SZA < 75°, residual errors from strong stratospheric photochemical gradients are effectively suppressed and estimated to be within 10%.

Consequently, the total estimated uncertainty for the retrieved VCDs during this ship-based campaign is approximately 18.1%–28.7%. Note that the relative uncertainty may increase when tropospheric concentrations are extremely low due to the pristine Arctic background. The uncertainty analysis is summarized in Table R2.

Table R2. MAX-DOAS retrievals uncertainty

Error sources	Estimated Uncertainty
Smoothing and Noise Error	5%-10%
Uncertainty of the reference spectrum	10%-15%
Algorithm Error	10%–20%
Errors from Stratospheric Gradient and Atmospheric Inhomogeneity	10%

The following content has been added:

Following established methodologies (Hendrick et al., 2007; Song et al., 2023; Tack et al., 2015; Wagner et al., 2007; Wittrock et al., 2004), the uncertainty in MAX-DOAS retrievals is categorized into four primary sources. First, smoothing and noise errors originate from statistical uncertainties in the DOAS fitting. Under clear-sky conditions, the fitting errors for NO_2, HCHO, BrO, and IO remain within 5% to 10%. Second, reference spectrum uncertainty arises because tropospheric DSCDs are determined by subtracting a sequential zenith reference spectrum (ZRS) from off-axis measurements. While this approach assumes stratospheric absorption cancels out, uncertainties in the residual trace gas abundances within the ZRS (stemming from stratospheric background or tropospheric pollution) can introduce systematic biases of approximately 10% to 15%. Third, algorithmic errors primarily stem from uncertainties in aerosol vertical distribution, multiple scattering simulations, and profile assumptions within the radiative transfer model. For the Arctic sea-ice environment, sensitivity tests demonstrate that surface albedo has a negligible impact on boundary layer observations at low elevation angles, with the total AMF uncertainty estimated at 10% to 20%. Fourth, residual errors from stratospheric gradients and atmospheric inhomogeneity are considered. By employing the sequential ZRS method and filtering for SZA < 75°, errors from steep stratospheric photochemical gradients are effectively suppressed to within 10%.

Consequently, the total uncertainty of the retrieved VCDs during this ship-borne campaign is estimated to be approximately 18.1% to 28.7%. Furthermore, due to the pristine background of the

Arctic region, the relative proportion of this uncertainty may increase when tropospheric concentrations are extremely low. Detailed information is provided in the Supplement.

Comment 6：

To address the reviewer's inquiry regarding the detection limits of different gases, we adopted two calculation strategies based on their photochemical properties and atmospheric distribution in the Arctic.

For NO_2, HCHO, and IO, which exhibit relatively clear tropospheric signals or minimal stratospheric interference, we employed the "2-sigma noise method" commonly used in the DOAS field (Chance and Spurr, 1997; Stutz and Platt, 1996; Wagner et al., 2007).

For BrO, considering its low tropospheric concentrations in the Arctic and the significant influence of the stratospheric BrO background, the conventional 2-sigma method may overestimate the tropospheric detection limit due to the excessive weighting of stratospheric absorption. Consequently, we followed the "equivalent RMS noise factor method" proposed by Coburn et al. (2011). This approach calculates the minimum identifiable slant column density by analyzing the root-mean-square (RMS) noise of the fit residuals at a given signal-to-noise ratio. The estimated detection limits for NO_2, HCHO, BrO, and IO during the observation period are 2.0 × 10^{15} molec.cm^{-2}, 5.0 × 10^{15} molec.cm^{-2}, 3.0 × 10^{13} molec.cm^{-2}, 1.3 × 10^{13} molec.cm^{-2}, respectively.

The following content has been added:

To evaluate the sensitivity of MAX-DOAS in the Arctic environment, different methods were adopted to calculate detection limits based on the atmospheric distribution and signal-to-noise ratio characteristics of various trace gases. First, for NO_2, HCHO, and IO, we used the standard method in DOAS applications to determine the detection limit (Chance and Spurr, 1997; Stutz and Platt, 1996; Wagner et al., 2007). The detection limit of the DSCD (LOD_{dSCD}) is defined as twice the statistical fitting error from the DOAS retrieval ($2\sigma_{fit}$). Second, for BrO, since tropospheric BrO concentrations in the Arctic are relatively low and influenced by the stratospheric BrO background, the conventional $2\sigma_{fit}$ noise method often over estimates the tropospheric detection limit because of the high weighting of stratospheric absorption. Therefore, we adopted the equivalent RMS noise factor method, which calculates the minimum identifiable slant column density at a given signal-to-noise ratio by analyzing the RMS noise of the residual spectrum (Coburn et al., 2011). During the observation period, the estimated detection limits for NO_2, HCHO, BrO, and IO were 2.0 × 10^{15} molec.cm^{-2}, 5.0 × 10^{15} molec.cm^{-2}, 3.0 × 10^{13} molec.cm^{-2}, 1.3 × 10^{13} molec.cm^{-2}, respectively.

Minor comments

It should be clearly stated whether the MAX-DOAS and satellite products represent tropospheric columns only or total columns (troposphere + stratosphere).

Re: Thank you for this comment.

We sincerely thank the reviewer for the thorough examination of the data definitions. The ship-based MAX-DOAS and satellite product data used in this study represent tropospheric column densities only. We have also added relevant content to clarify this in the revised

manuscript.

The following content has been added:

Ship-based MAX-DOAS retrieves differential slant column densities (DSCDs) using sequential zenith reference spectra, which effectively eliminates the stratospheric background and enables the detection of tropospheric trace gases.

This study compares ship-based MAX-DOAS measurements with tropospheric VCD products from multiple satellite instruments, including the Tropospheric Monitoring Instrument (TROPOMI), Geostationary Environmental Monitoring Spectrometer (GEMS), and Global Ozone Monitoring Experiment-2 (GOME-2).

At several points (Lines 37, 71, 79, 110, 118, 520, 537), MAX-DOAS is referred to as an in situ measurement. MAX-DOAS is a remote sensing technique and should be described as such.

Re: Thank you for this comment.

We are grateful to the reviewer for identifying this terminological oversight. We recognize that the use of "in-situ" was technically imprecise, given that MAX-DOAS is a remote sensing technique rather than a point-source measurement. To ensure technical accuracy, we have replaced all instances of "in-situ" with "ship-based MAX-DOAS" throughout the revised manuscript. This adjustment clarifies the path-integrated nature of our observations as opposed to localized sampling.

The following content has been added:

1). By filling critical observational gaps in the Arctic marine boundary layer, this study verifies established RHS source mechanisms and offers high-resolution ship-based MAX-DOAS observations as prior constraints for atmospheric chemistry models. These empirical data can be directly utilized to refine polar emission parameterizations and reactive halogen budgets, significantly enhancing the fidelity of models such as GEOS-Chem and WRF-Chem in simulating polar atmospheric processes and improving the reliability of global climate assessments.

2). Ground-based stations deliver high resolution ship-based DOAS data but are predominantly located in terrestrial or island regions of Antarctica and the Arctic.

3). By filling critical observational gaps in the Arctic marine boundary layer, this report provides essential empirical constraints for upgrading the parameterizations of halogen chemical cycles in atmospheric chemistry models (e.g., GEOS-Chem and WRF-Chem), thereby enhancing the accuracy of polar air – sea interaction simulations and global climate assessments.

Line 128: Is 169.18°W intended to be 169.18°E?

Re: Thank you for this comment.

We are very grateful to the reviewer for the meticulous review. The coordinate 169.18°W is the correct value.

Our cruise track covers both Eastern and Western longitudes. Specifically, when the research vessel was located in the Eastern Hemisphere (near 169.18°E), it was still in low-latitude open seas without sea ice. However, when entering the Western Hemisphere (including 169.18°W), the vessel had advanced to high-latitude regions within the Arctic sea-ice zone.

Section 2.2.1: It would be useful to discuss uncertainties associated with separating tropospheric

and stratospheric contributions using DSCDs, particularly in the presence of sharp stratospheric gradients.

Re: Thank you for this comment.

We appreciate the reviewer's professional advice regarding the uncertainty in separating stratospheric and tropospheric contributions, which is a key technical challenge for MAX-DOAS observations at high latitudes. To address this, we followed the measures taken in previous studies (Hong et al., 2018; Tack et al., 2015; Wagner et al., 2007; Xing et al., 2023).

1). Differential retrieval using sequential zenith reference spectra: During the retrieval process, each set of off-axis observations was analyzed using its temporally adjacent zenith observation as a reference. The physical assumption is that because the measurement interval is very short and the solar zenith angle (SZA) change is minimal, the light paths and corresponding absorption in the stratosphere are nearly identical. Most of the stratospheric background is canceled through this subtraction, allowing for the extraction of tropospheric signals.

2). Data filtering criteria (SZA < 75°): We only retained spectra with SZA smaller than 75°. Strong stratospheric gradients mainly originate from the rapid photochemical evolution at sunrise or sunset, particularly for NO_2 and BrO. Under the condition of SZA < 75°, stratospheric photochemistry remains in a quasi-steady state with relatively smooth concentration changes.

3). Cancellation of geometric paths: At low SZA, the difference in the stratospheric light path between 10°/20° elevation angles and the 90° zenith angle is small. By calculating the difference, the majority of the stratospheric signal is effectively canceled.

Finally, following previous error assessments (Hendrick et al., 2007; Tack et al., 2015; Wittrock et al., 2004), the uncertainty introduced by stratospheric inhomogeneity is generally well-constrained during the day. By excluding the highly variable twilight periods, the total estimated retrieval error for this high-latitude campaign ranges from 11.2% to 14.1%.

The following content has been added:

The separation of tropospheric and stratospheric contributions using DSCDs involves several layers of uncertainty. Following established error assessment methodologies (Hendrick et al., 2007; Tack et al., 2015; Wittrock et al., 2004), the total uncertainty in our retrieved tropospheric vertical columns is attributed to two primary factors. First, spectral noise and statistical fitting uncertainties account for approximately 5% to 10% of the DSCD error under clear-sky conditions. Second, uncertainties arise from atmospheric spatial inhomogeneity and stratospheric photochemical gradients. These gradients are particularly pronounced for reactive species such as NO_2 and BrO. To mitigate this, we restricted our analysis to observations with SZA < 75°, ensuring that the stratosphere remained in a photochemical quasi-steady state. Additionally, the implementation of a sequential zenith reference spectrum (ZRS) within short intervals (a few minutes) effectively minimizes the influence of stratospheric temporal and spatial variability. In the Arctic environment, the residual error stemming from stratospheric gradients following the sequential ZRS subtraction is estimated to be less than 10%.

Based on these components, the combined uncertainty for the tropospheric and stratospheric separation during this campaign ranges from 11.2% to 14.1%. We note that the relative uncertainty may increase in the pristine Arctic atmosphere when tropospheric abundances are near detection limits.

Lines 201–203: A surface albedo of 0.06 is reasonable for open ocean but likely too low for sea ice. Please justify the parameter choices and indicate whether sensitivity tests were performed to demonstrate that these assumptions do not significantly affect the results.

Re: Thank you for this comment.

We appreciate the reviewer's constructive advice regarding the characterization of surface albedo. To quantify the sensitivity of our retrieval at elevation angles of 10°, 20°, and 90°, we conducted radiative transfer simulations using SCIATRAN (v2.1). The model utilized the Henyey-Greenstein scattering phase function combined with the delta-M approximation (truncation index of 34). Aerosol properties were defined using high-latitude profiles representative of the Arctic environment, with a slit function HWHM of 0.5 nm. Assuming that halogen species are predominantly located within the planetary boundary layer, we simulated tropospheric AMFs across an albedo range of 0.06 to 0.8 (Figure R12). Our results indicate that the relative deviation in AMF remains below 5% for all considered elevation angles.

Although the zenith geometry is more significantly affected by surface reflection, this systematic bias is further canceled out when calculating the differential $\Delta AMF(AMF_{10°/20°} - AMF_{90°})$. This is because we typically utilize the zenith observation as the reference spectrum for calculating DSCDs, which allows the shared reflection-induced offsets to be subtracted.

$$\frac{|AMF_{0.8} - AMF_{0.06}|}{AMF_{0.06}} \times 100\% \quad (6)$$

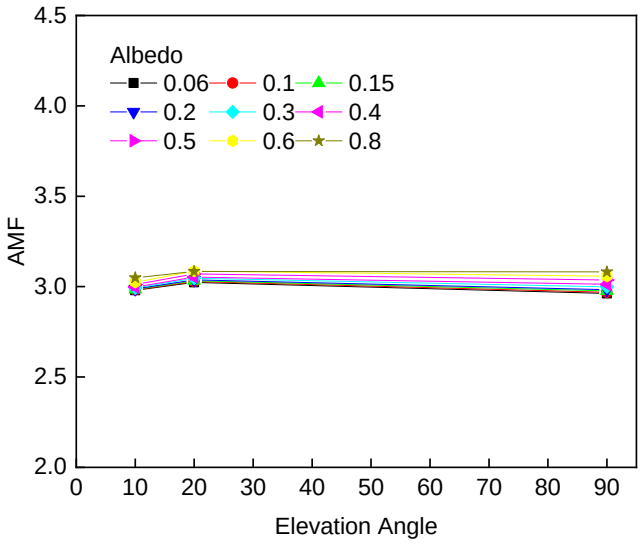

Figure R12. Sensitivity of simulated AMF to different surface albedo values.

Consistent with established MAX-DOAS theory (Frieß et al., 2001, 2016; Hönninger et al., 2004), the effective optical path at low elevation angles is predominantly controlled by atmospheric scattering along the telescope's line of sight. Under these conditions, the geometric path length dominates, while the contribution of surface-reflected radiation to the total radiance remains minor. For halogen species such as BrO and IO residing within the planetary boundary layer, the majority of the absorption occurs during the atmospheric scattering process before the photons interact with the surface. Consequently, the retrieval of these boundary-layer species exhibits minimal sensitivity to uncertainties or changes in surface albedo.

Several figures are missing labels for color scales, and overall font sizes are too small. Increasing

font size would improve readability.

Re: Thank you for this comment.

We appreciate the reviewer's meticulous scrutiny and constructive feedback concerning the quality of our illustrations. Following these recommendations, we have revised all figures throughout the manuscript to enhance their clarity and overall presentation. These adjustments ensure that all graphical data are presented in a manner consistent with the journal's high standards.

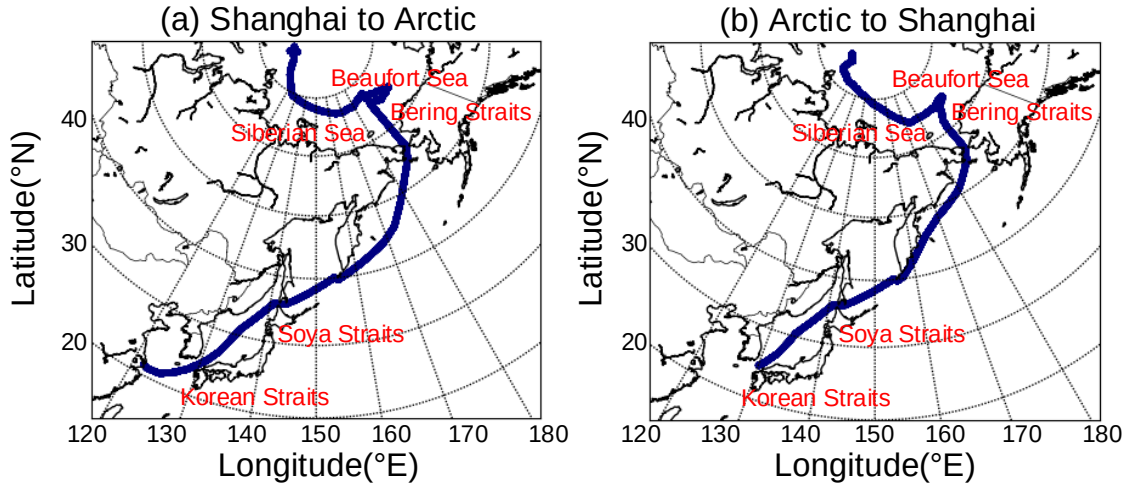

Fig R13. Trajectories of the research vessel for the 12th Arctic Scientific Expedition: (a) Go from Shanghai to the Arctic; (b) Return from the Arctic

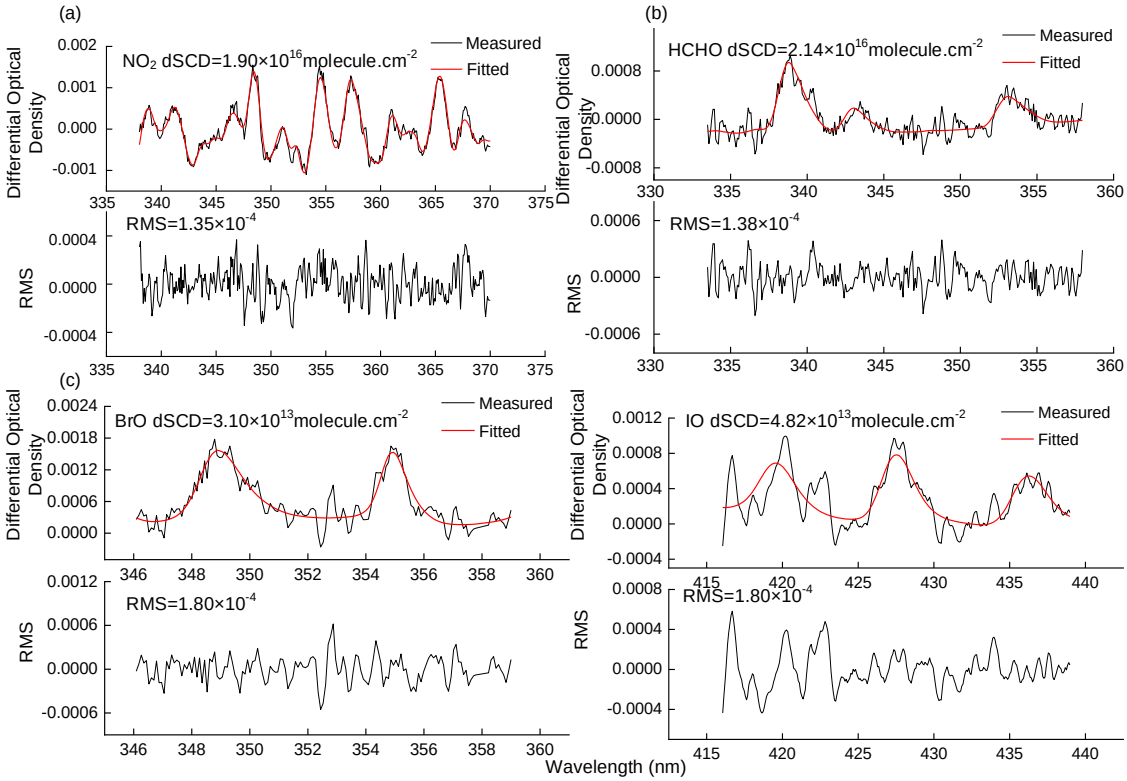

Fig R14. An example of Ship MAX-DOAS spectral fittings for (a) NO_2, (b) HCHO, (c) BrO, and (d) IO. The spectrum was recorded at 1：02 UTC on August 15, 2021, with an elevation 10°.

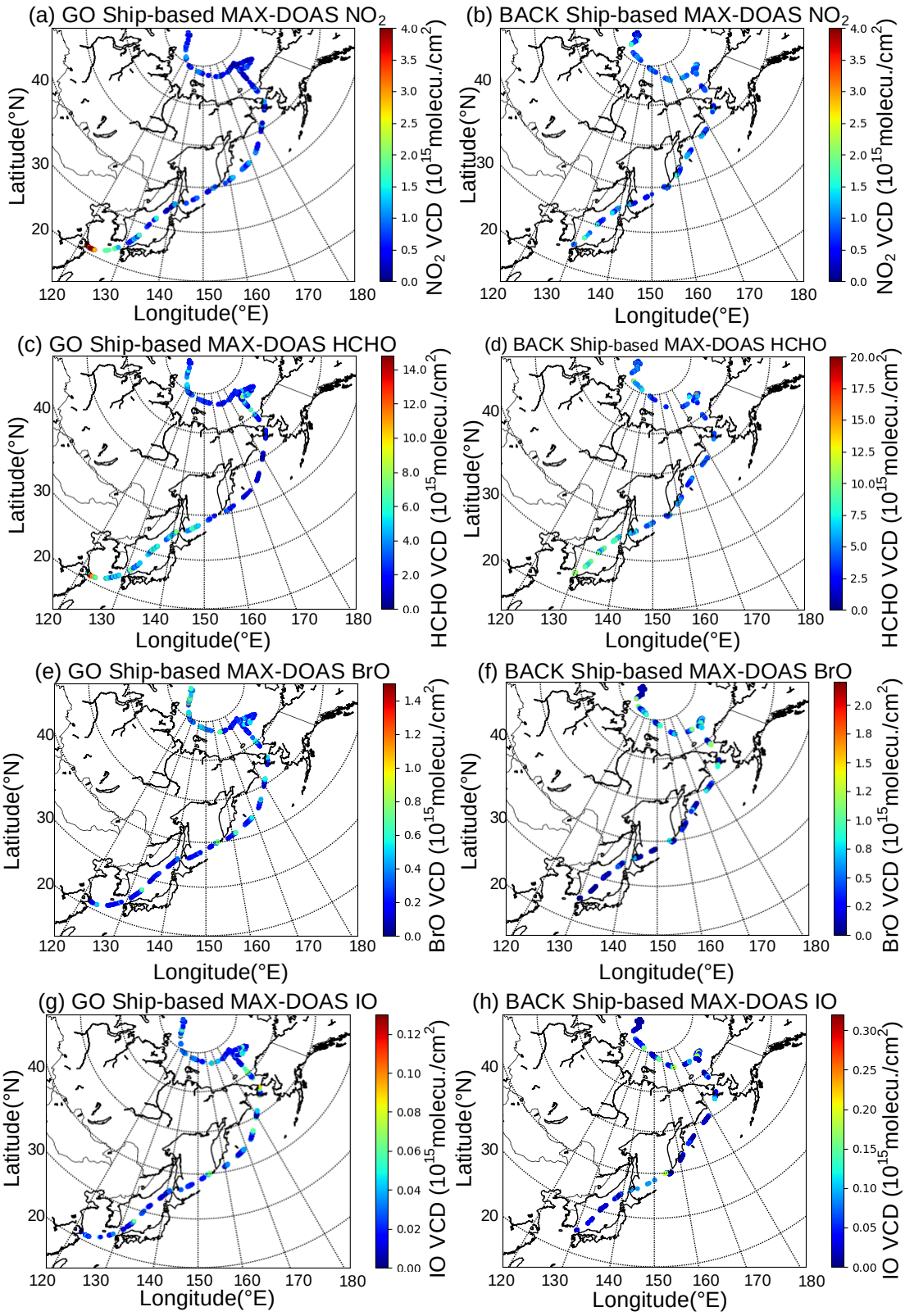

Fig R15. Spatial distributions of pollutants (NO_2, HCHO, BrO, and IO) VCDs.

Panels (a), (c), (e), (g) present NO_2, HCHO, BrO, and IO distributions along the go route from Shanghai to the Arctic, while panels (b), (d), (f), (h) show their distributions along the return route from the Arctic to Shanghai.

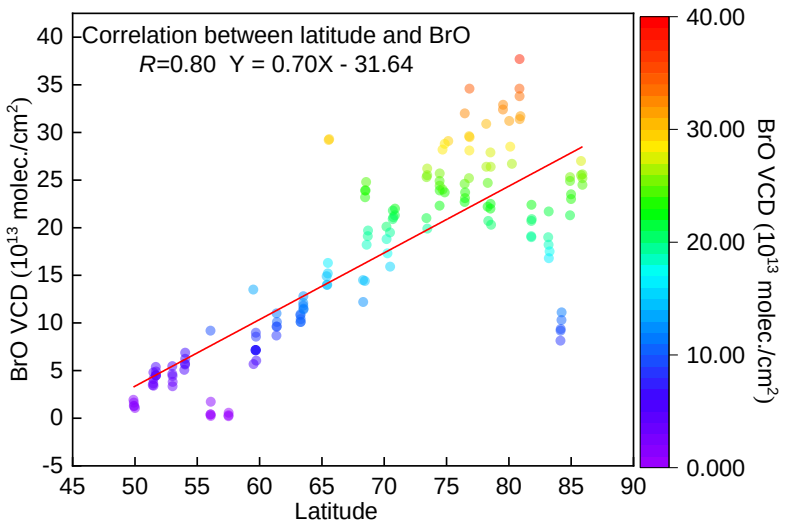

Fig R16. BrO concentration variation observed by ship-based MAX-DOAS with latitude

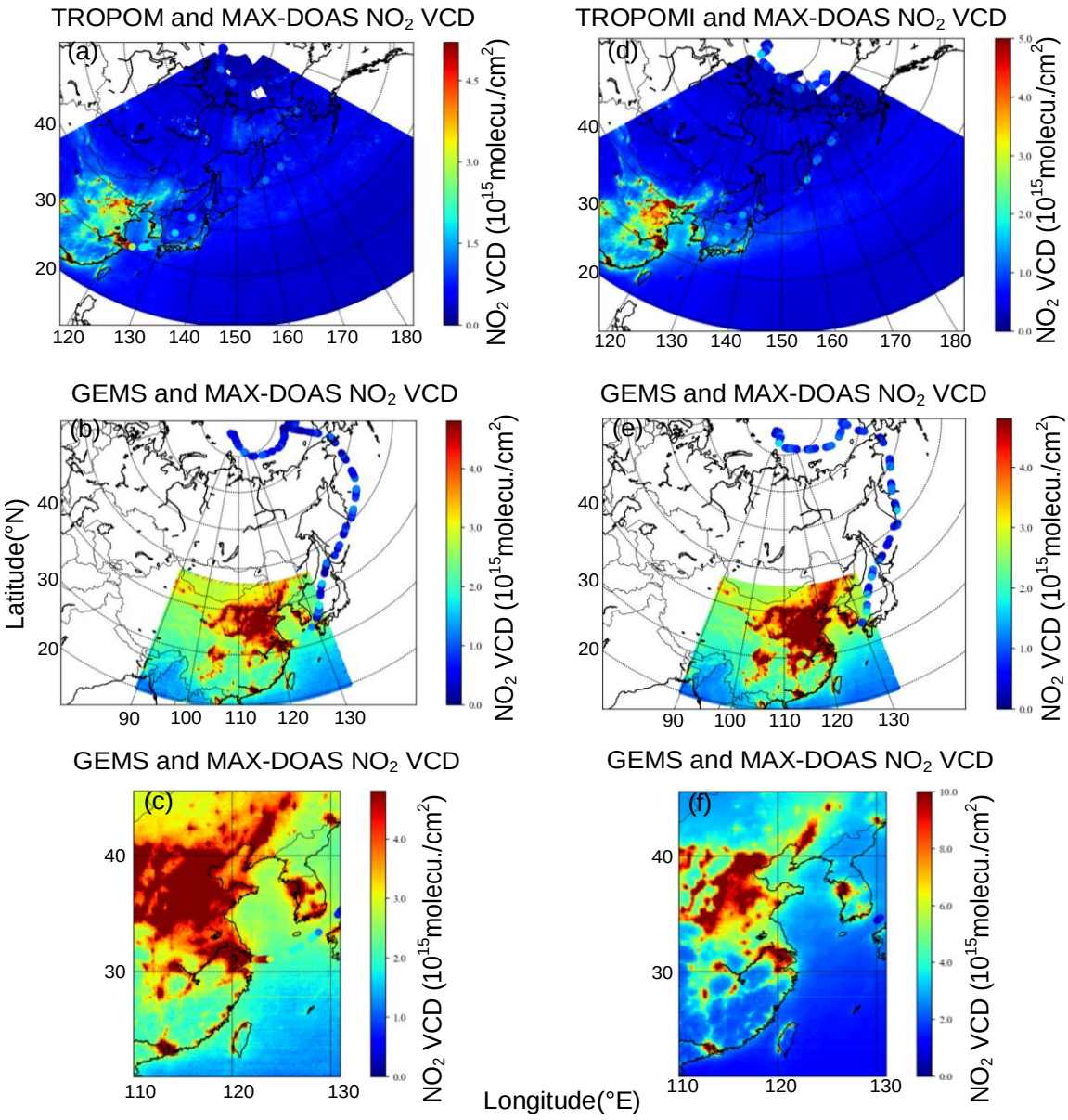

Fig R17. Comparison of ship-based MAX-DOAS measured NO_2 VCDs with satellite observations: (a-c) Shanghai to Arctic and (d-f) Arctic to Shanghai.

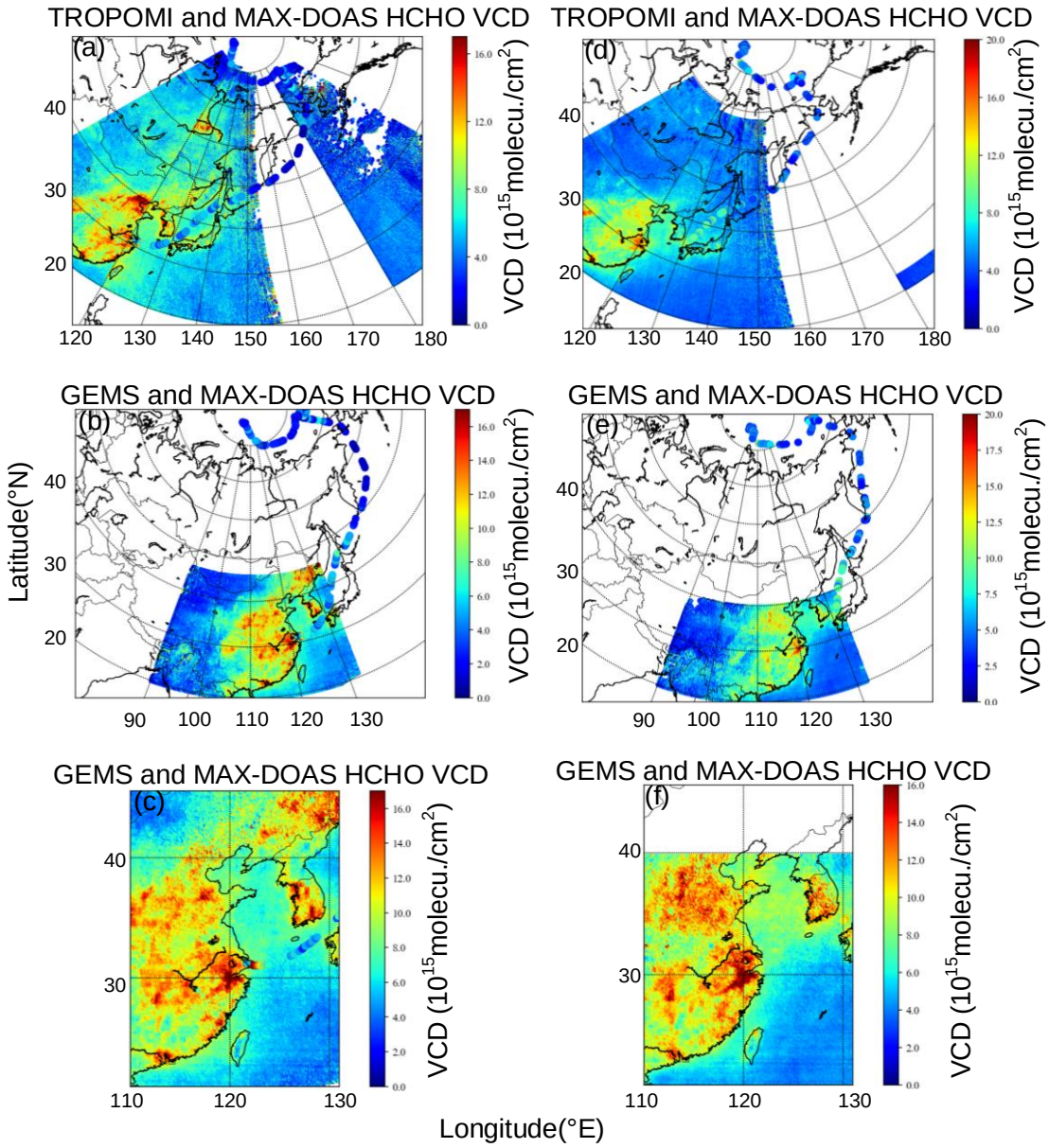

Fig R18. Comparison of ship-based MAX-DOAS measured HCHO VCDs with satellite observations: (a-c) Shanghai to Arctic and (d-f) Arctic to Shanghai.

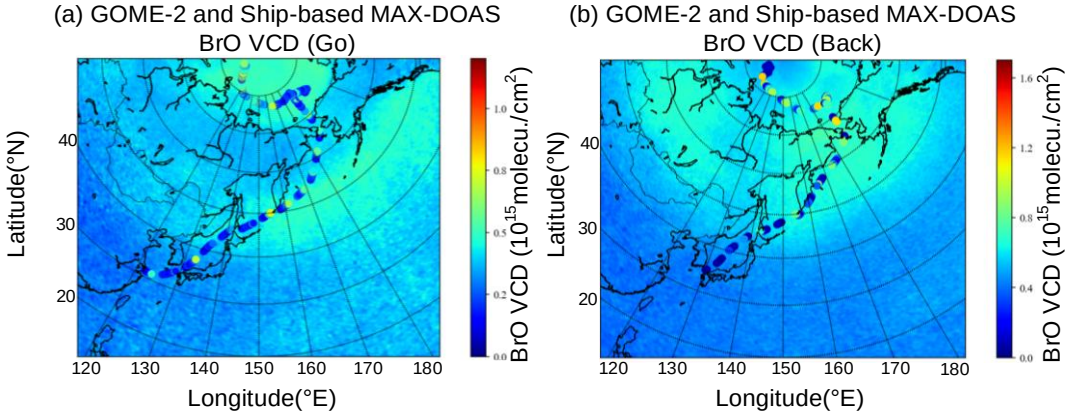

Fig R19. Comparison of ship-based MAX-DOAS measured BrO VCDs with GOME-2 observations: (a) Shanghai to Arctic and (b) Arctic to Shanghai.

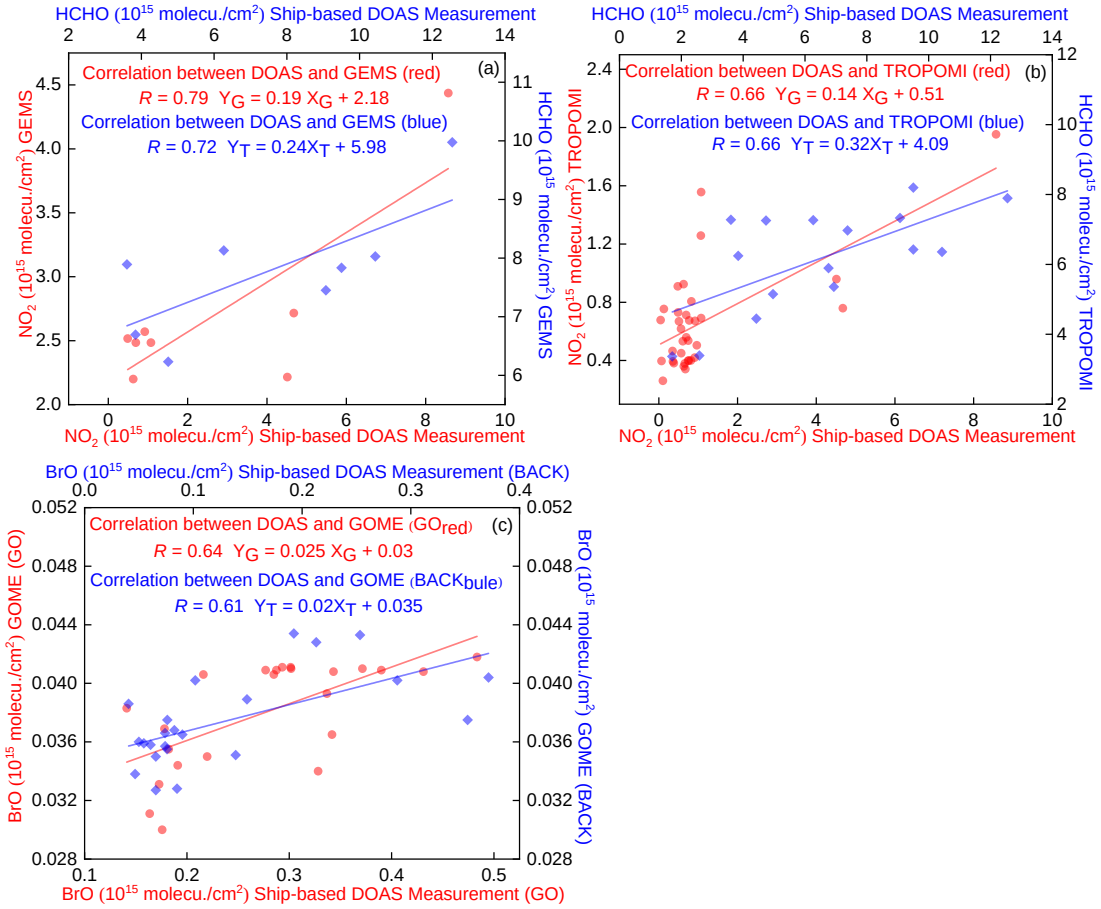

Fig R20. Correlation analysis between daily measurements and satellite observations during the ship-based campaign. Panels (a) GEMS, (b) TROPOMI, (c) GOME-2.

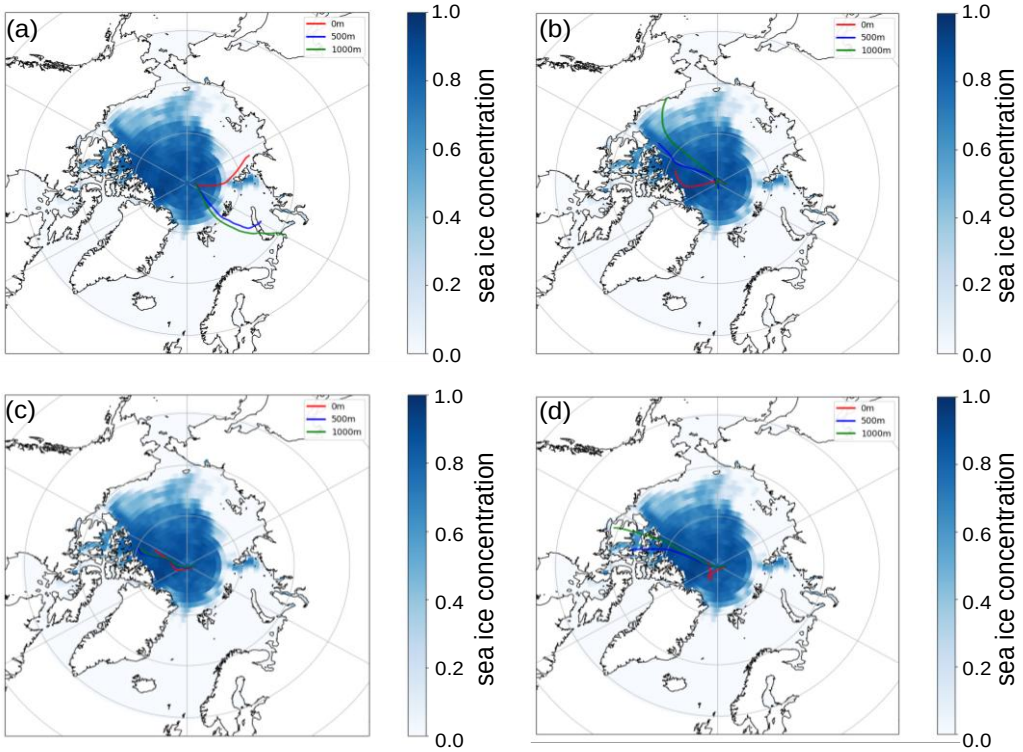

Fig R 21. Backward trajectories of polluted air masses at the target site overlaid on Arctic sea-ice concentration (August 2021)

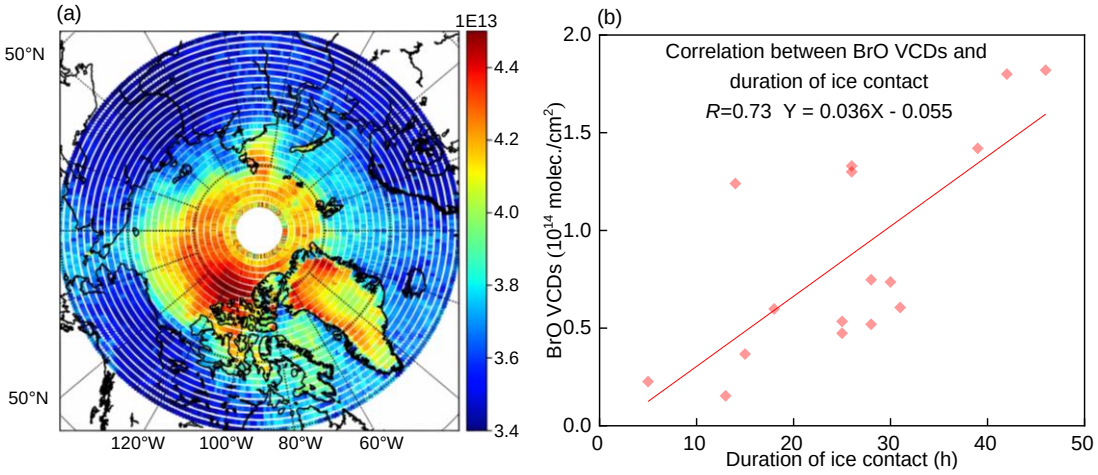

Fig R 22. Source region characteristics of Arctic BrO. (a) GOME-2 derived spatial distribution of BrO VCDs. (b) Correlation between air mass sea ice contact duration and ship-based BrO VCDs

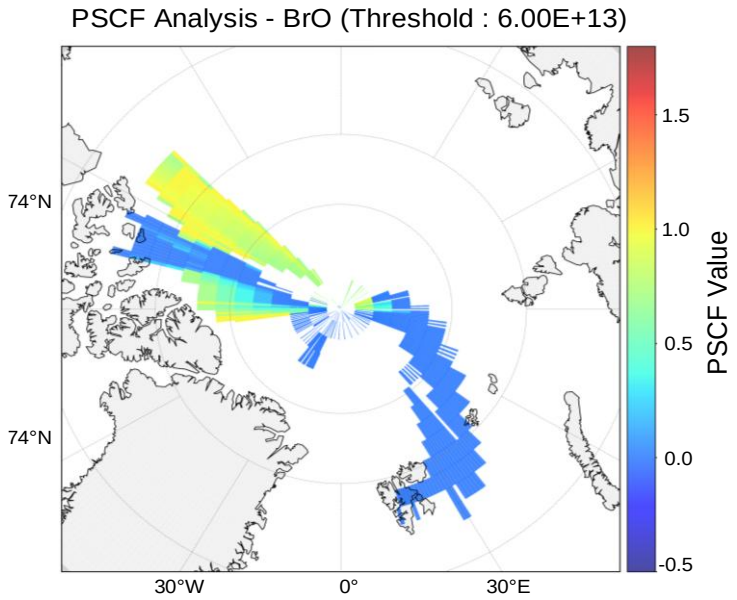

Fig R 23. PSCF analysis for BrO in the Arctic

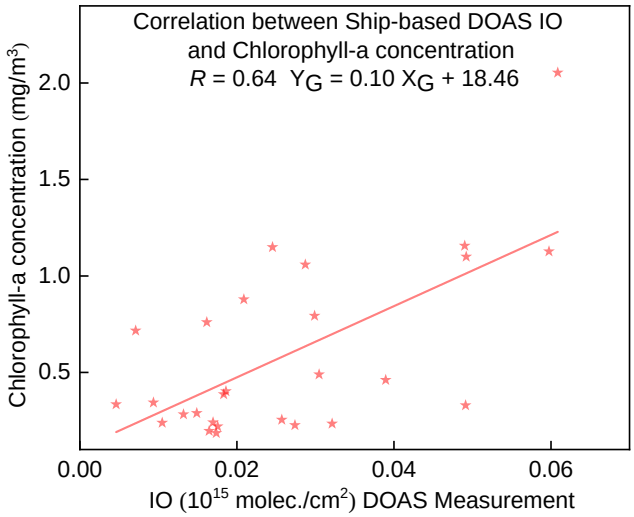

Fig R 24. Correlation between ship-based IO VCDs and Chlorophyll-a

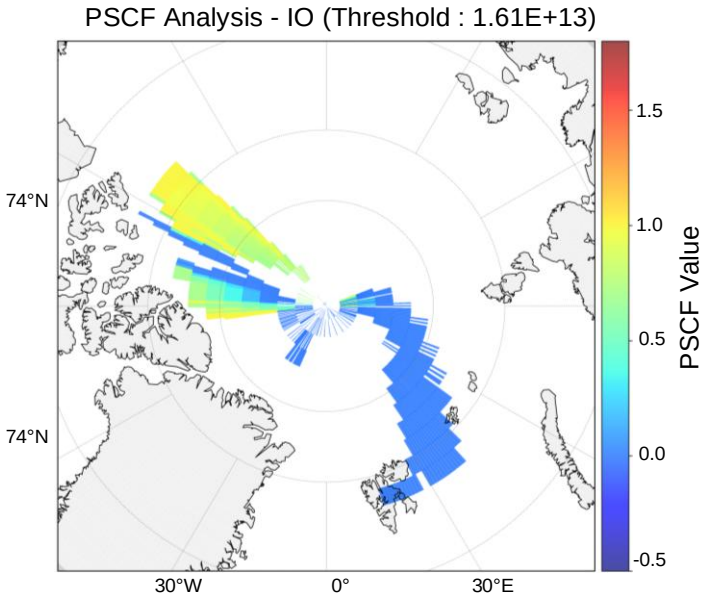

Fig R 25. PSCF analysis for IO in the Arctic

Throughout the manuscript, BrO and IO are referred to as “pollutants” or “pollution.” As reactive halogens are not pollutants in the traditional sense, alternative terminology is recommended.

Re: Thank you for this comment.

We appreciate the reviewer's insightful comment concerning the precision of our terminology. We agree that BrO and IO, as naturally occurring constituents of the polar atmosphere, are distinct from conventionally defined pollutants. To ensure scientific rigor, we have revised the manuscript to employ the collective designation "trace gases" for NO_2, HCHO, BrO, and IO. This adjustment accurately reflects the chemical nature of these species within the context of the natural Arctic halogen cycle.

The following content has been added:

1. Fig. 3 presents the spatial distributions of VCDs of four trace gases during the cruise (round trip from Shanghai to the Arctic).

2. The high value regions of different trace gases exhibit distinct regional variations: NO_2 and HCHO VCD maxima are concentrated in low latitude areas with intensive anthropogenic activities, with the highest concentrations observed in the Shanghai Port region.
3. This gridding process not only preserves the true spatial distribution of trace gases but also retains details of pollution hotspots (e.g., ports, shipping lanes), avoiding comparison biases from spatial scale mismatch.
4. Satellites have substantially lower spatial resolution than ship-based MAX-DOAS point scale measurements and are less sensitive to local trace gas sources.
5. This leads to slightly higher ship-based observations compared to satellite retrievals in trace gas intensive regions (e.g., ports, shipping lanes).
6. During mobile measurements, the ship's exhaust plume could interfere with trace gas measurements under unfavorable wind conditions.

Line 424: PSCF should be spelled out at first mention. A brief description of the PSCF method should also be added to the methods section, including whether weighting was applied based on air mass residence frequency within each grid cell.
Re: Thank you for this comment.

We appreciate the reviewer's constructive feedback. In the revised manuscript, we have provided the full definition of the Potential Source Contribution Function (PSCF) and included a brief description in the methodology section.

Specifically, the PSCF value for a grid cell (i, j) is defined as the ratio of trajectory endpoints associated with concentrations exceeding a specific threshold ($m_{i,j}$) to the total number of endpoints falling within that cell ($n_{i,j}$). To mitigate the statistical instability and uncertainty inherent in grid cells with a limited number of endpoints, we incorporated a piecewise weighting function ($n_{i,j}$). This approach, resulting in the Weighted PSCF (WPSCF), effectively minimizes small sample bias and ensures the reliability of the identified source regions.

The following content has been added:

The PSCF is a Lagrangian receptor-oriented model employed to pinpoint potential emission source areas. For a specific grid cell (i, j), the PSCF value is defined as the ratio of the number of "polluted" trajectory endpoints ($m_{i,j}$), associated with concentrations exceeding a predefined threshold) to the total number of endpoints ($n_{i,j}$) residing in that cell.

$$\mathrm{PSCF_{ij}} = \frac{\mathrm{m_{ij}}}{\mathrm{n_{ij}}} \tag{9}$$

To reduce uncertainty caused by small grid counts, this study refers to Pernov et al., (2021);, Polissar et al., (2001), Yin et al., (2018)by introducing a weight function to obtain the weighted PSCF (WPSCF). The formula is as follows:

$$\mathrm{WPSCF_{i,j}} = \mathrm{W(n_{ij})} \times \mathrm{PSCF_{i,j}}$$

$$\mathrm{W(n_{ij})} = \begin{cases} 1.00 & \mathrm{n_{ij}} > \mathrm{n_{avg}} \\ 0.70 & \mathrm{n_{avg}}/3 < \mathrm{n_{ij}} \le \mathrm{n_{avg}} \\ 0.42 & \mathrm{n_{avg}}/5 < \mathrm{n_{ij}} \le \mathrm{n_{avg}}/3 \\ 0.17 & \mathrm{n_{ij}} \le \mathrm{n_{avg}}/5 \end{cases} \tag{10}$$

Where n_{avg} represents the average number of endpoints across all grid cells.

Reference

Abbatt, J. P. D., Thomas, J. L., Abrahamsson, K., Boxe, C., Granfors, A., Jones, A. E., King, M. D., Saiz-Lopez, A., Shepson, P. B., Sodeau, J., Toohey, D. W., Toubin, C., von Glasow, R., Wren, S. N., and Yang, X.: Halogen activation via interactions with environmental ice and snow in the polar lower troposphere and other regions, Atmospheric Chemistry and Physics, 12, 6237-6271, https://doi.org/10.5194/acp-12-6237-2012, 2012.

Bognar, K., Zhao, X., Strong, K., Chang, R. Y. W., Frieß, U., Hayes, P. L., McClure-Begley, A., Morris, S., Tremblay, S., and Vicente-Luis, A.: Measurements of Tropospheric Bromine Monoxide Over Four Halogen Activation Seasons in the Canadian High Arctic, Journal of Geophysical Research: Atmospheres, 125, e2020JD033015, https://doi.org/10.1029/2020JD033015, 2020.

Brockway, N., Peterson, P. K., Bigge, K., Hajny, K. D., Shepson, P. B., Pratt, K. A., Fuentes, J. D., Starn, T., Kaeser, R., Stirm, B. H., and Simpson, W. R.: Tropospheric bromine monoxide vertical profiles retrieved across the Alaskan Arctic in springtime, Atmospheric Chemistry and Physics, 24, 23-40, https://doi.org/10.5194/acp-24-23-2024, 2024.

Burd, J. A., Peterson, P. K., Nghiem, S. V., Perovich, D. K., and Simpson, W. R.: Snowmelt onset hinders bromine monoxide heterogeneous recycling in the Arctic, Journal of Geophysical Research: Atmospheres, 122, 8297–8309, https://doi.org/10.1002/2017JD026906, 2017.

Chance, K. V. and Spurr, R. J. D.: Ring effect studies: Rayleigh scattering, including molecular parameters for rotational Raman scattering, and the Fraunhofer spectrum, Applied Optics., AO, 36, 5224-5230, https://doi.org/10.1364/AO.36.005224, 1997.

Coburn, S., Dix, B., Sinreich, R., and Volkamer, R.: The CU ground MAX-DOAS instrument: characterization of RMS noise limitations and first measurements near Pensacola, FL of BrO, IO, and CHOCHO, Atmospheric Measurement Techniques, 4, 2421–2439, https://doi.org/10.5194/amt-4-2421-2011, 2011.

Domine, F., Albert, M., Huthwelker, T., Jacobi, H.-W., Kokhanovsky, A. A., Lehning, M., Picard, G., and Simpson, W. R.: Snow physics as relevant to snow photochemistry, Atmospheric Chemistry and Physics, 8, 171–208, https://doi.org/10.5194/acp-8-171-2008, 2008.

Eicken, H., Krouse, H. R., Kadko, D., and Perovich, D. K.: Tracer studies of pathways and rates of meltwater transport through Arctic summer sea ice, Journal of Geophysical Research (Oceans), 107, 8046, https://doi.org/10.1029/2000JC000583, 2002.

Frey, M. M., Norris, S. J., Brooks, I. M., Anderson, P. S., Nishimura, K., Yang, X., Jones, A. E., Nerentorp Mastromonaco, M. G., Jones, D. H., and Wolff, E. W.: First direct observation of sea salt aerosol production from blowing snow above sea ice, Atmospheric Chemistry and Physics, 20, 2549–2578, https://doi.org/10.5194/acp-20-2549-2020, 2020.

Frieß, U., Wagner, T., Pundt, I., Pfeilsticker, K., and Platt, U.: Spectroscopic measurements of tropospheric iodine oxide at Neumayer Station, Antarctica, Geophysical Research Letters, 28, 1941–1944, https://doi.org/10.1029/2000GL012784, 2001.

Frieß, U., Hollwedel, J., König-Langlo, G., Wagner, T., and Platt, U.: Dynamics and chemistry of tropospheric bromine explosion events in the Antarctic coastal region, Journal of Geophysical Research: Atmospheres, 109, https://doi.org/10.1029/2003JD004133, 2004.

Frieß, U., Sihler, H., Sander, R., Pöhler, D., Yilmaz, S., and Platt, U.: The vertical distribution of BrO and aerosols in the Arctic: Measurements by active and passive differential optical absorption spectroscopy, Journal of Geophysical Research: Atmospheres, 116, https://doi.org/10.1029/2011JD015938, 2011.

Frieß, U., Klein Baltink, H., Beirle, S., Clémer, K., Hendrick, F., Henzing, B., Irie, H., de Leeuw, G., Li, A., Moerman, M. M., van Roozendael, M., Shaiganfar, R., Wagner, T., Wang, Y., Xie, P., Yilmaz, S., and Zieger, P.: Intercomparison of aerosol extinction profiles retrieved from MAX-DOAS measurements, Atmospheric Measurement Techniques, 9, 3205-3222, https://doi.org/10.5194/amt-9-3205-2016, 2016.

Hara, K., Osada, K., Matsunaga, K., Iwasaka, Y., Shibata, T., and Furuya, K.: Atmospheric inorganic chlorine and bromine species in Arctic boundary layer of the winter/spring, Journal of Geophysical Research: Atmospheres, 107, AAC 4-1-AAC 4-15, https://doi.org/10.1029/2001JD001008, 2002.

Hara, K., Osada, K., Yabuki, M., Takashima, H., Theys, N., and Yamanouchi, T.: Important contributions of sea-salt aerosols to atmospheric bromine cycle in the Antarctic coasts, Scientific Reports, 8, 13852, https://doi.org/10.1038/s41598-018-32287-4, 2018.

Hendrick, F., Van Roozendael, M., Chipperfield, M. P., Dorf, M., Goutail, F., Yang, X., Fayt, C., Hermans, C., Pfeilsticker, K., Pommereau, J.-P., Pyle, J. A., Theys, N., and De Mazière, M.: Retrieval of stratospheric and tropospheric BrO profiles and columns using ground-based zenith-sky DOAS observations at Harestua, 60 deg; N, Atmospheric Chemistry and Physics, 7, 4869-4885, https://doi.org/10.5194/acp-7-4869-2007, 2007.

Hong, Q., Liu, C., Chan, K. L., Hu, Q., Xie, Z., Liu, H., Si, F., and Liu, J.: Ship-based MAX-DOAS measurements of tropospheric NO_2, SO_2, and HCHO distribution along the Yangtze River, Atmospheric Chemistry and Physics, 18, 5931–5951, https://doi.org/10.5194/acp-18-5931-2018, 2018.

Hönninger, G., von Friedeburg, C., and Platt, U.: Multi axis differential optical absorption spectroscopy (MAX-DOAS), Atmospheric Chemistry and Physics, 4, 231–254, https://doi.org/10.5194/acp-4-231-2004, 2004.

Hurlock, S. C., Stutz, J., von Glasow, R., and Piot, M.: DOAS Measurements of Reactive Halogens at Greenland Summit in May and June, 2007, AGU Fall Meeting Abstracts, ADS Bibcode: 2007AGUFM.A51C0581H, A51C-0581, 2007.

Jacobi, H.-W., Morin, S., and Bottenheim, J. W.: Observation of widespread depletion of ozone in the springtime boundary layer of the central Arctic linked to mesoscale synoptic conditions, Journal of Geophysical Research: Atmospheres, 115, https://doi.org/10.1029/2010JD013940, 2010.

Luo, Y., Si, F., Zhou, H., Dou, K., Liu, Y., and Liu, W.: Observations and source investigations of the boundary layer bromine monoxide (BrO) in the Ny-Ålesund Arctic, Atmospheric Chemistry and Physics, 18, 9789–9801, https://doi.org/10.5194/acp-18-9789-2018, 2018.

May, N. W., Quinn, P. K., McNamara, S. M., and Pratt, K. A.: Multiyear study of the dependence of sea salt aerosol on wind speed and sea ice conditions in the coastal Arctic, JGR Atmospheres, 121, 9208–9219, https://doi.org/10.1002/2016JD025273, 2016.

Moore, C. W., Obrist, D., Steffen, A., Staebler, R. M., Douglas, T. A., Richter, A., and Nghiem, S. V.: Convective forcing of mercury and ozone in the Arctic boundary layer induced by leads in sea ice, Nature, 506, 81–84, https://doi.org/10.1038/nature12924, 2014.

Nilsson, E. D., Rannik, Ü., Swietlicki, E., Leck, C., Aalto, P. P., Zhou, J., and Norman, M.: Turbulent aerosol fluxes over the Arctic Ocean: 2. Wind-driven sources from the sea, Journal of Geophysical Research, 106, 32,139-32,154, https://doi.org/10.1029/2000JD900747, 2001.

Peng, S., Yang, Q., Shupe, M. D., Xi, X., Han, B., Chen, D., Dahlke, S., and Liu, C.: The

characteristics of atmospheric boundary layer height over the Arctic Ocean during MOSAiC, Atmospheric Chemistry and Physics, 23, 8683–8703, https://doi.org/10.5194/acp-23-8683-2023, 2023.

Pernov, J. B., Bossi, R., Lebourgeois, T., Nøjgaard, J. K., Holzinger, R., Hjorth, J. L., and Skov, H.: Atmospheric VOC measurements at a High Arctic site: characteristics and source apportionment, Atmospheric Chemistry and Physics, 21, 2895–2916, https://doi.org/10.5194/acp-21-2895-2021, 2021.

Peterson, P. K., Pöhler, D., Sihler, H., Zielcke, J., General, S., Frieß, U., Platt, U., Simpson, W. R., Nghiem, S. V., Shepson, P. B., Stirm, B. H., Dhaniyala, S., Wagner, T., Caulton, D. R., Fuentes, J. D., and Pratt, K. A.: Observations of bromine monoxide transport in the Arctic sustained on aerosol particles, Atmospheric Chemistry and Physics, 17, 7567–7579, https://doi.org/10.5194/acp-17-7567-2017, 2017.

Pinardi, G., Van Roozendael, M., Hendrick, F., Theys, N., Abuhassan, N., Bais, A., Boersma, F., Cede, A., Chong, J., Donner, S., Drosoglou, T., Dzhola, A., Eskes, H., Frieß, U., Granville, J., Herman, J. R., Holla, R., Hovila, J., Irie, H., Kanaya, Y., Karagkiozidis, D., Kouremeti, N., Lambert, J.-C., Ma, J., Peters, E., Piters, A., Postylyakov, O., Richter, A., Remmers, J., Takashima, H., Tiefengraber, M., Valks, P., Vlemmix, T., Wagner, T., and Wittrock, F.: Validation of tropospheric NO_2 column measurements of GOME-2A and OMI using MAX-DOAS and direct sun network observations, Atmospheric Measurement Techniques, 13, 6141–6174, https://doi.org/10.5194/amt-13-6141-2020, 2020.

Polissar, A. V., Hopke, P. K., and Harris, J. M.: Source regions for atmospheric aerosol measured at Barrow, Alaska, Environ Sci Technol, 35, 4214–4226, https://doi.org/10.1021/es0107529, 2001.

Pratt, K. A., Custard, K. D., Shepson, P. B., Douglas, T. A., Pöhler, D., General, S., Zielcke, J., Simpson, W. R., Platt, U., Tanner, D. J., Gregory Huey, L., Carlsen, M., and Stirm, B. H.: Photochemical production of molecular bromine in Arctic surface snowpacks, Nature Geosci, 6, 351–356, https://doi.org/10.1038/ngeo1779, 2013.

Richter, A., Wittrock, F., Eisinger, M., and Burrows, J. P.: GOME observations of tropospheric BrO in northern hemispheric spring and summer 1997, Geophysical Research Letters, 25, 2683–2686, https://doi.org/10.1029/98GL52016, 1998.

Roberts, T. J., Jourdain, L., Griffiths, P. T., and Pirre, M.: Re-evaluating the reactive uptake of HOBr in the troposphere with implications for the marine boundary layer and volcanic plumes, Atmospheric Chemistry and Physics, 14, 11185–11199, https://doi.org/10.5194/acp-14-11185-2014, 2014.

Seo, S., Richter, A., Blechschmidt, A.-M., Bougoudis, I., and Burrows, J. P.: Spatial distribution of enhanced BrO and its relation to meteorological parameters in Arctic and Antarctic sea ice regions, Atmospheric Chemistry and Physics, 20, 12285–12312, https://doi.org/10.5194/acp-20-12285-2020, 2020.

Shupe, M. D., Persson, P. O. G., Brooks, I. M., Tjernström, M., Sedlar, J., Mauritsen, T., Sjogren, S., and Leck, C.: Cloud and boundary layer interactions over the Arctic sea ice in late summer, Atmospheric Chemistry and Physics, 13, 9379–9399, https://doi.org/10.5194/acp-13-9379-2013, 2013.

Simpson, W. R., Carlson, D., Hönninger, G., Douglas, T. A., Sturm, M., Perovich, D., and Platt, U.: First-year sea-ice contact predicts bromine monoxide (BrO) levels at Barrow, Alaska better than potential frost flower contact, Atmospheric Chemistry and Physics, 7, 621–627,

https://doi.org/10.5194/acp-7-621-2007, 2007.
Simpson, W. R., Peterson, P. K., Frieß, U., Sihler, H., Lampel, J., Platt, U., Moore, C., Pratt, K., Shepson, P., Halfacre, J., and Nghiem, S. V.: Horizontal and vertical structure of reactive bromine events probed by bromine monoxide MAX-DOAS, Atmospheric Chemistry and Physics, 17, 9291–9309, https://doi.org/10.5194/acp-17-9291-2017, 2017.
Song, Y., Xing, C., Liu, C., Lin, J., Wu, H., Liu, T., Lin, H., Zhang, C., Tan, W., Ji, X., Liu, H., and Li, Q.: Evaluation of transport processes over North China Plain and Yangtze River Delta using MAX-DOAS observations, Atmospheric Chemistry and Physics, 23, 1803–1824, https://doi.org/10.5194/acp-23-1803-2023, 2023.
Stutz, J. and Platt, U.: Numerical analysis and estimation of the statistical error of differential optical absorption spectroscopy measurements with least-squares methods, Appl. Opt., AO, 35, 6041–6053, https://doi.org/10.1364/AO.35.006041, 1996.
Swanson, W. F., Graham, K. A., Halfacre, J. W., Holmes, C. D., Shepson, P. B., and Simpson, W. R.: Arctic Reactive Bromine Events Occur in Two Distinct Sets of Environmental Conditions: A Statistical Analysis of 6 Years of Observations, Journal of Geophysical Research: Atmospheres, 125, e2019JD032139, https://doi.org/10.1029/2019JD032139, 2020.
Tack, F., Hendrick, F., Goutail, F., Fayt, C., Merlaud, A., Pinardi, G., Hermans, C., Pommereau, J.-P., and Van Roozendael, M.: Tropospheric nitrogen dioxide column retrieval from ground-based zenith–sky DOAS observations, Atmospheric Measurement Techniques, 8, 2417–2435, https://doi.org/10.5194/amt-8-2417-2015, 2015.
Theys, N., Van Roozendael, M., Hendrick, F., Yang, X., De Smedt, I., Richter, A., Begoin, M., Errera, Q., Johnston, P. V., Kreher, K., and De Mazière, M.: Global observations of tropospheric BrO columns using GOME-2 satellite data, Atmospheric Chemistry and Physics, 11, 1791–1811, https://doi.org/10.5194/acp-11-1791-2011, 2011.
Tremblay, S., Picard, J.-C., Bachelder, J. O., Lutsch, E., Strong, K., Fogal, P., Leaitch, W. R., Sharma, S., Kolonjari, F., Cox, C. J., Chang, R. Y.-W., and Hayes, P. L.: Characterization of aerosol growth events over Ellesmere Island during the summers of 2015 and 2016, Atmospheric Chemistry and Physics, 19, 5589–5604, https://doi.org/10.5194/acp-19-5589-2019, 2019.
Wagner, T., Ibrahim, O., Sinreich, R., Frieß, U., von Glasow, R., and Platt, U.: Enhanced tropospheric BrO over Antarctic-sea ice in mid-winter observed by MAX-DOAS on board the research vessel Polarstern, Atmospheric Chemistry and Physics, 7, 3129–3142, https://doi.org/10.5194/acp-7-3129-2007, 2007.
Wittrock, F., Oetjen, H., Richter, A., Fietkau, S., Medeke, T., Rozanov, A., and Burrows, J. P.: MAX-DOAS measurements of atmospheric trace gases in Ny-Ålesund - Radiative transfer studies and their application, Atmospheric Chemistry and Physics, 4, 955–966, https://doi.org/10.5194/acp-4-955-2004, 2004.
Xing, C., Xu, S., Song, Y., Liu, C., Liu, Y., Lu, K., Tan, W., Zhang, C., Hu, Q., Wang, S., Wu, H., and Lin, H.: A new insight into the vertical differences in NO_2 heterogeneous reaction to produce HONO over inland and marginal seas, Atmospheric Chemistry and Physics, 23, 5815–5834, https://doi.org/10.5194/acp-23-5815-2023, 2023.
Yin, X., Kang, S., de Foy, B., Ma, Y., Tong, Y., Zhang, W., Wang, X., Zhang, G., and Zhang, Q.: Multi-year monitoring of atmospheric total gaseous mercury at a remote high-altitude site (Nam Co, 4730 m a.s.l.) in the inland Tibetan Plateau region, Atmospheric Chemistry and Physics, 18, 10557–10574, https://doi.org/10.5194/acp-18-10557-2018, 2018.